Comments to the Author from Editor Jennifer Hutchings

Thank you very much for your detailed response to the reviewers comments. There are still some concerns that need to be addressed before this paper is suitable for publication in The Cryosphere. Please consider the further comments of reviewer 1. Importantly, the paper could benefit from professional English proof reading.

Reply: The latest major revised manuscript has been checked by a native English speaker.

I would like to see more clarity in your argument that pond color is related to ice thickness beneath the pond. In particular, you have no quantitative discussion on the dependence of this relationship on your assumptions for optical properties of the ice.

Reply: We have given the relationship between pond color vector (r, g, b intensities) and ice thickness (H_i) and pond depth (H_p) in Fig. 4 (c-e) using the default values of incident solar radiation F_0 and ice optical properties.

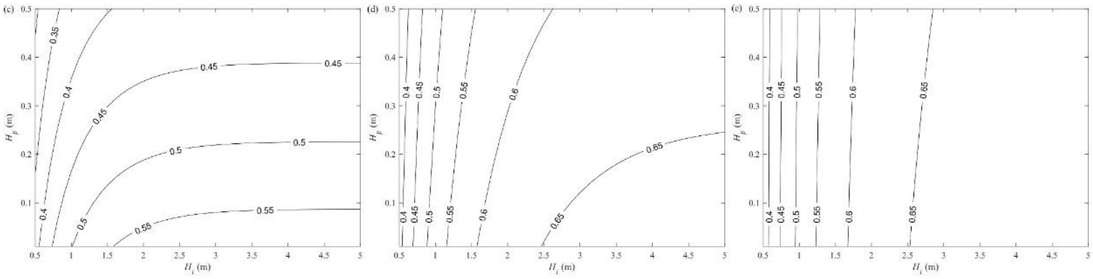

Figure 4. Variations of melt-pond color with pond depth H_p and underlying ice thickness H_i using default values of F_0 and ice optical properties. (c–e) denote intensities of red, green, and blue components scaled in the range of 0–1.

The dependence of the relationship on ice optics is only investigated for a typical case of H_i = 1 m and H_p = 0.3 m using the model (see Fig. 7 in the manuscript). Such dependence can be extended for a large range of H_i and H_p as given below. Now if we change the value of F_0 from the default value to another possible value in summer Arctic according to Fig. 5a in the manuscript, we can get the variations in the pond color resulted from varying F_0 as comparing with Fig. 4 (c-e). The results are shown in Fig. S1.

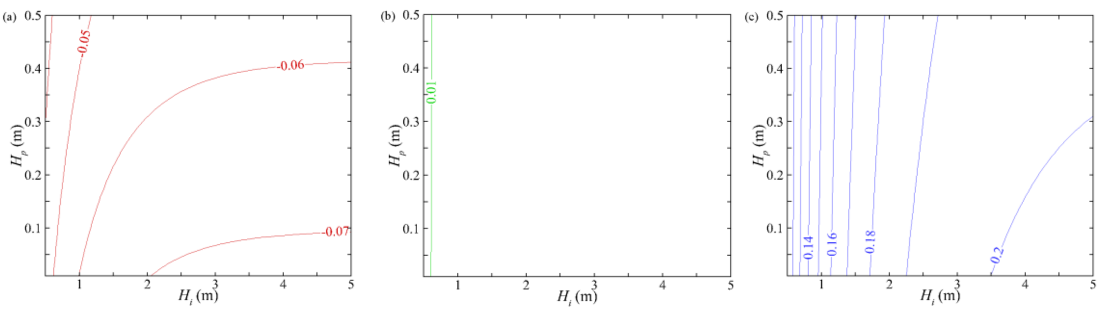

Figure S1. Variations in the (a) r, (b) g, (c) b intensities if we only change F_0, from August 7 to September 10 (Fig. 5a in the manuscript) as comparing with the default results of pond color shown in Fig. 4 (c-e).

Similarly, if we only change ice scattering coefficient σ_i, the resulted difference in pond color is shown in Fig. S2. And if ice absorption coefficient $k_{\lambda,i}$ is altered, the difference in pond color is also shown in Fig. S3. In principle, the model works with non-dimensional absorption and scattering parameters $H_i \cdot \sigma_i$ and $H_i \cdot k_{\lambda,i}$ and $H_p \cdot k_{\lambda,w}$ and errors in the absorption and scattering coefficients bring corresponding errors to estimated ice thickness. Since the main uncertainty is in the scattering coefficient and scattering is the governing process in attenuation of radiation in ice, in the first order, the relative error of r % in the scattering coefficient causes relative error of r % to the estimated ice thickness.

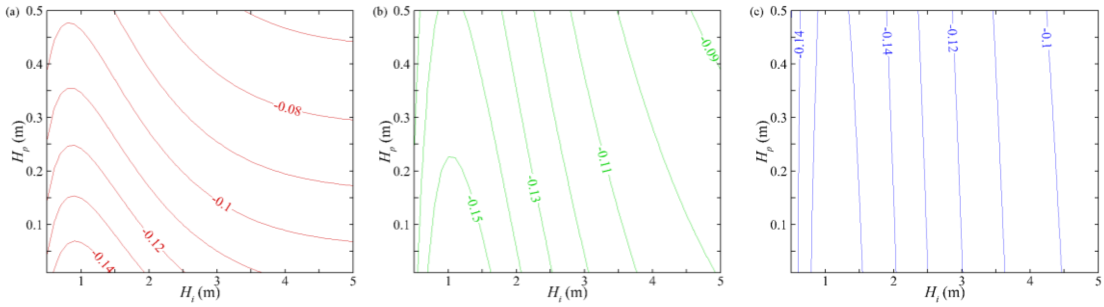

Figure S2. Variations in the (a) r, (b) g, (c) b intensities if we only change σ_i, from 2.5/m to 1.2/m, as comparing with the default results of pond color shown in Figure 4 (c-e).

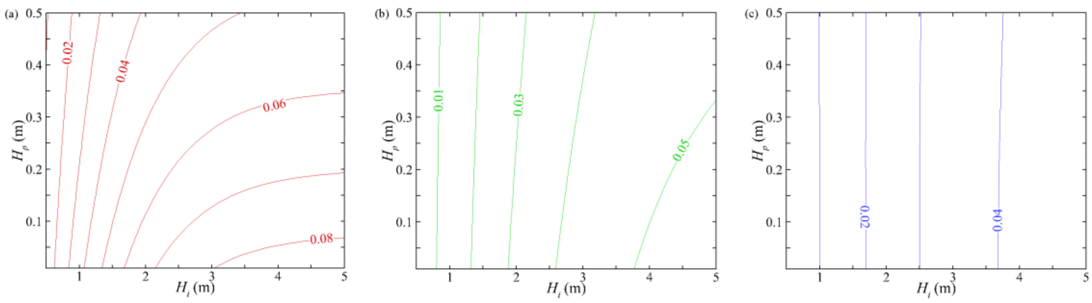

Figure S3. Variations in the (a) r, (b) g, (c) b intensities if we only change $k_{\lambda,i}$, from max. to min. (Figure 3 in the manuscript) as comparing with the default results of pond color shown in Figure 4 (c-e).

We can see the impact of F_0 on the relationship between pond color and H_i and H_p in Fig. S1. As the value of F_0 changes from the default value of August 7 to September 10 (lowest level in Fig. 5a), the red intensity decreases by at most 0.07, and the green intensity is nearly constant, and the blue intensity increases by at most 0.2. The variation trend is similar with that in Fig. 5b, and the resulted variation is only significant in the blue intensity for very thick ice (H_i > 3 m) as comprising with Fig. 4 (c-e).

In Fig. S2, as ice scattering coefficient σ_i changes from 2.5/m to 1.2/m, the red intensity decreases by at most 0.14, and the green and blue intensities decrease by at most 0.15. The resulted difference in pond color is large for thin ice and small for thick ice in Fig. S2. It can be explained by the impotant role of scattering in ice on the upwelling irradiance from pond surface for thin ice. For thick ice, most irradiance have been dissapated due to absorption in ice, and any further changes in scattering coefficient or ice thickness will not change the upwelling irradiance very much. This has been discussed in Lu et al. (2016).

In Fig. S3, although the absorption coefficient of sea ice changes from its maximum to minimum (cf. Fig. 3 in the mannuscript), the resulted variations in pond color are below 0.08, similar with the results of Fig. 7b. That is, the influence of ice absroption on pond color can be ignored.

These three figures (Figs. S1-S3) gave the impacts of F_0 and ice optical properties on the relationship between pond color and H_i, H_p. And they are results for all possible values of H_i and H_p, not for a typical case of H_i = 1 m, and H_p = 0.3 m, whose results are shown in the Fig. 5a, Fig. 7a, and Fig. 7b, respectively in the manuscript.

Figs. S1-S3 are not included in the revised manuscript to avoid any further complexity and difficulties. But the illustrated outcome is explained verbally in the text, and we combined the results of Figs. S1-S3 with the revised Fig. 9 in the manuscript, and we added the errors in simulated pond color due to different selections of the values of F_0 and ice optical properties. Please see the reply to the comments on Fig. 9 below.

Abstract: Note the comments from reviewer 1. If pond color is not related to Hi, you can not claim this here. Further in the manuscript you identify that the relationship is only true for ice thinner than 1m. This is important to include in the abstract, if it is indeed true.
Reply: We made our argument clear in the revised manuscript, i.e. the pond color has a certain relationship with the sea ice thickness below melt pond when less than 1 m.

Page 1 line 9: Capitalize 'using' Please check your grammer throughout.
Reply: This sentence is: "Pond color, which creates the visual appearance of melt ponds on Arctic sea ice in summer, is quantitatively investigated using a two-stream radiative transfer model for ponded sea ice.".

Page 1, line 25: " lower the surface albedo from as high as 0.8 (snow) to as low as 0.15" strange grammer. rephrase.
Reply: This sentence is rephrased to: "lower the surface albedo from 0.8 (snow) to 0.15 (pond)".

" As a result, melt ponds are an issue as important and inevitable as the dramatic decay of current Arctic sea ice". I don't understand this. Melt ponds are not the issue. You need to rephrase this sentence, or change it for something that makes sense.
Reply: This sentence is rephrased to: "melt ponds play an important role on the dramatic decay of current Arctic sea ice cover (Flocco et al., 2012)".

page 2, line 28: clarify what are trapped ponds?
Reply: The word "trapped ponds" is replaced by "refrozen ponds".

page 3: " Efforts will also be made to find ways to use the information provided by pond color more effectively because this color contains the optical response of melt ponds and sea ice

to incident solar radiation. " an example of a sentence that needs work. First of all, do you want to use the future tense here, perhaps more specifically state "in this paper" and the sentence is convoluted. It is not easy to understand.
Reply: We rephrased the sentence to: "Efforts are also made to find ways to effectively use the information provided by pond color.".

page 4, line 20: again check grammer, remove "and". Please get some professional help in correcting your English.
Reply: The manuscript has been checked by a native English speaker.

page 5, title for section 2.2. From which spectrum? clarify. Perhaps 'observed spectrum'?
Reply: We revised the title to "Estimation of pond color from simulated upwelling spectrum".

page 5: Illuminance Y, and the Y coordinate can be confused. Please consider using different symbols.
Reply: Illuminance Y is actually the value of a color on the Y coordinate in the XYZ color space defined by CIE. To avoid any confusion, we revised the "XYZ coordinates" to "XYZ tristimulus values".

page 7, line 9: "... melt pond albedo is sensitive to Hi for thin ice, but to Hp for thick ice, ..." This sentence does not make sense, is one property (Hi, Hp) sensitive and the other is not?
Reply: When sea ice thickness was below 1.5 m, melt pond albedo was sensitive to the ice thickness and the sensitivity was not affected by the melt pond depth. When sea ice is getting thicker (> 1.5 m), the melt pond albedo is no more sensitive to the ice thickness. We changed the sentence to "the melt-pond albedo depends mainly on H_i for thin ice (H_i < 1.5 m), and on H_p for thick ice (H_i > 1.5 m)".

page 10, line 15: "The agreement is acceptable". In order to make this statement you need to know the sensitivity of hue, saturation and luminance to sky conditions and ice optical properties. I see that you have numerical experiments considering both optical properties of the ice and solar zenith angle, so I expect you can provide some numbers for the sensitivity so we can believe your statement. It is not possible to determine this sensitivity from the manuscript because you only provide a plot (figure 7) of the sensitivity of pond color to optical properties for 1m ice. I need to be able to see that the sensitivity to ice optical properties does not larger than the variation shown in figure that will allow depth to be estimated to a reasonable tolerance for the result to be meaningful. In figure 7 the range of scattering coefficient results in pond colors that are over a larger range than the observations shown in figure 4. What is a reasonable range for the uncertainty in scattering, and how does this impact the results presented in figure 4. (And the same question for other parameters in the model).
Reply: We revised Fig. 9 and added a new paragraph to tell the uncertainty in pond color due to different values of ice optical properties and incident radiation.

The questions on Figs. 4 and 7 can be addressed by Figs. S1-S3 above, where they are not only for H_i = 1 m but for all possible values of H_i and H_p. And in the first order, the system works with non-dimensional optical absorption and scattering lengths H·k and H·σ so that the relative accuracy is proportional to the relative accuracy of the governing optical parameters.

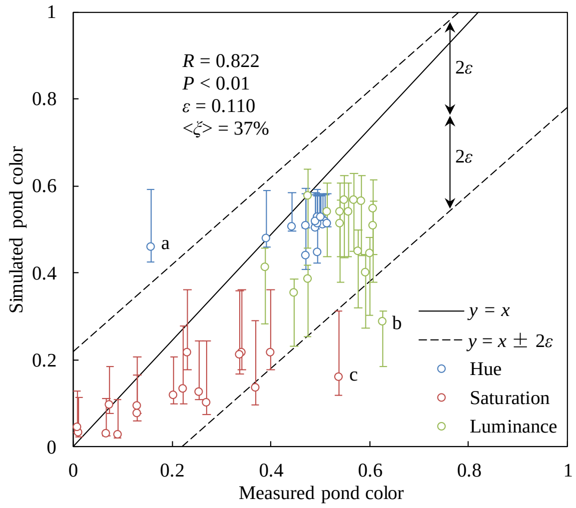

Figure 9: Comparisons of simulated pond color with in-situ measurements by Istomina et al. (2016) in the HSL color space. Points a, b, and c are special cases discussed in the text. The vertical error bars on the simulated color denote the uncertainties due to variations in the incident solar radiation and ice scattering coefficient different from their default values. R is the correlation coefficient between simulated and measured color. P is the significance level of the correlation. ε is the root-mean-square error, and <ξ> is the mean of relative error in simulated color.

"H_i and H_p are changing variables in the calculation. Uncertainties, among others, are the different in-situ conditions, such as sky conditions and ice optical properties, which need to be specified in the model since these in-situ properties were not measured in Istomina et al. (2016). We therefore carried out sensitivity studies by altering the values of F_0, σ_i, and $k_{\lambda,i}$ within reasonable ranges for Arctic sea ice in summer to reveal their impacts on the simulated pond color. The negative error bars in the simulated values in Fig.9 are associated with the scattering in ice as σ_i drops from the default value (2.5 m^{-1}) to 1.2 m^{-1} (Fig. 7a). The positive error bars are induced by F_0 as it decreases from the representative data in August to low levels in September (Fig. 5a). The influence of ice absorption coefficient on the simulated pond color is very limited (< 0.02), similar with Fig. 5b, and therefore not included in the error bars. It is revealed on Fig.9 that the impact of σ_i on the hue and saturation values is less than 0.05, and that on the luminance is less than 0.14. On the contrary, variation in the luminance value due to F_0 is less than 0.04, and that in the hue and saturation is less than 0.15. That is, the maximum uncertainty in the simulated hue, saturation, and luminance values will not exceed 0.2 for different combinations of incident solar radiation and IOPs for summer sea ice. More importantly, these variations still locate almost within the range of ± 2ε, namely the 95% confidence interval (Fig. 9). In other words, these experiments underline the importance of H_i and H_p in determining the color of melt ponds compared with other impact factors."

page 11, line 11: I do not think "Besides" should be hear. The ice scattering and the water scattering are separate from each other in the context of this discussion.

Reply: We revised the sentence to: “It is also assumed here that melt pond water is clean and scattering can be neglected”.

page 14, line 10: "The result is acceptable because of the very few available data here". Few data points is rarely a reason for a result to be acceptable! There is correlation between the data sets, I would just state the facts and leave out subjective sentences like this one.

Reply: Removed the sentence accordingly.

page 14, line 13: "The results give support for a possible new way method of determining the sea-ice thickness, especially for melting sea ice," In order for this to be true the method needs to have sufficient fidelity to provide meaningful thickness estimates. i.e. what is the resolution of thickness, for thin ice below 1m thick, that could be resolved with the method? Is this resolution a function of thickness, lighting conditions?

Reply: We understand the point, but the resolution and its variations may be difficult to see, because as we have said in the text that the available data is very few (they are only 5 points in the range H_i < 1m, figure 10b). What we want to do in the paper is just to reveal the relationship between pond color and ice thickness. The relationship is solid at least from the statistics of available data at this moment, and this suggests a possibility of ice thickness retrieve. But a robust method of ice thickness retrieve need more field observations. We have stated at the end of the manuscript that further study, especially the *in-situ* measurements are urgently needed in order to validate our method and eventually make the methodology able to resolve the different ice thickness classification on the basis of pond color.

page 16, line 10-15. Very long sentence. Break up in to a least two sentences.

Reply: The sentence is rephrased to: “In comparison, retrieval of ice thickness from pond color has an obvious advantage over all other methods. Hand-held, ship-borne or airborne photography of melt ponds, especially widespread UAVs equipped with a digital camera, is easy to perform during field campaigns.”.

page 16, line 17-18: "As the first insight into the color of melt ponds, we tend to pose a possibility instead of draw a conclusion because of the limited available observations so far". "tend to pose" is vague and makes the reader think you are not clear on the future direction. I recommend you rephrase this sentence.

Reply: We rephrased the sentence to: “The possibility of a color-retrieval method was explored in this study using the limited available observations so far.”.

Please ensure your figure numbering is correct in the text in relation to the changed figure numbers? I am not sure figure 9 is referred to correctly. Do you have significance and correlation values for both figures 9 and 10? Are you actually improving correlation by taking the small subset of data with Hi < 1m?

Reply: All figure numbers in the text are checked again.

Yes, Figure 9 is correctly referred in the text.

Yes, the statistical parameters are now included in both Figs. 9 and 10.

Yes, the correlation is improved by taking the subset data with H_i < 1m.

Figures are missing panel labels. Please place (a), (b) etc appropriately.

Reply: The panel labels are included in Figures 2, 4, 5, 7, and 10 who have subfigures.

If you need any clarification on these comments, please do not hesitate to contact me to set up a time to talk by phone.

Very best regards,

Jenny

Comments from Anonymous Referee #1

The authors have completed sufficient revisions to address the concerns raised in my review of the earlier draft. I have a few minor comments on the current draft:

p. 3 line 23-25. "Albedo sensed by spectral radiometers represents the spectrum upwelling irradiance from the surface,…" Well, no, albedo is the ratio of upwelling to downwelling irradiance, it really tells nothing explicitly about the upwelling irradiance. Also, phrase "spectrum upwelling" makes no sense. It is true that the color of a pond is the response of the human eye, and it is true that the upwelling irradiance does depend on the reflected radiation from the pond surface, and the backscattered radiation from the ice and water below. But, not sure why these things are all in the same sentence. This sentence needs to be rewritten.

Reply: This sentence was revised to: "The color of a melt pond is the response of human eyes to the upwelling irradiance from the surface, which consists of the reflected solar radiation from the pond surface and the backscattering radiation from ice and water below.".

P4 line 20: I don't know the word "illuminant"

Reply: "illuminant" refers to the source of light according to the International Commission on Illumination (usually abbreviated CIE for its French name).

p6 line 17-18: "A value of σ i = 2.5 m -1 has been promoted by LU16 for summer Arctic sea ice." Is that to say that the authors intend to hold the scattering coefficient for the ice beneath ponds constant? The reason for stating this scattering coefficient should be explained.

Reply: Yes, the scattering coefficient of sea ice is constant except for the sensitivity study of σ_i in section 3.3. The reason of selecting the value is explained now. (1) The values of scattering coefficient for eight types of sea ice and snow have been investigated in Perovich (1990), from 0 for bubble-free ice to 800 m^{-1} for cold dry snow. (2) Sensitivity studies conducted in Lu et al. (2016) have revealed that the value of σ_i = 2.5 m^{-1} can produce a more comparable melt-pond albedo with field observations than other value of σ_i. So a value of σ_i = 2.5 m^{-1} is also employed in this study.

p6 line 24-25: Pond depth and ice thickness do affect pond albedo and color, but I think the other, perhaps most important, factor is the characteristic scattering of the ice immediately beneath the pond. The analysis later in the manuscript gets around to this point, but I think that idea should be described here.

Reply: We rephrased the sentence to: "The color of a melt pond changes with different factors such as sky conditions, ice properties, and pond depth (Light et al., 2015; Istomina et al., 2016). We investigate the influence of various factors on pond color in the following sections.".

P7 line 8 -9: "Basically, melt ponds on FYI in Arctic are shallow and flat, resulting in various gray color tones, while MYI melt ponds are always deep and narrow, displaying green and blue…" I think this is as result of different pond depths, yes, different ice thickness, yes, but additionally, of different characteristic scattering properties in the FY and MY ice. Also, ponds on MY ice are not necessarily deep and narrow at the beginning of the summer melt season.

Reply: We changed to "Basically, melt ponds on FYI in Arctic are shallow and flat, resulting in various gray color tones, while melt ponds on MYI may have relative larger depth ranges and more complex geometrical patterns, displaying green and blue."

And in the discussion of ice scattering coefficient in section 3.3, we added "Additionally, MYI in Arctic contains much less brine and more gas bubbles than FYI, then the more scattering in MYI is another possible factor causing the different color of melt ponds on MYI and FYI except for Hi and Hp (Fig. 4f).".

P8 line 12: "…sea ice from melting blue ice…" would be clearer if "…sea ice ranging from melting blue ice…"

Reply: Corrected accordingly.

The color of melt ponds on Arctic sea ice

Peng Lu[1], Matti Leppäranta[2], Bin Cheng[3], Zhijun Li[1], Larysa Istomina[4], Georg Heygster[4]

[1]State Key Laboratory of Coastal and Offshore Engineering, Dalian University of Technology, Dalian, 116024, China
[2]Institute of Atmospheric and Earth Sciences, University of Helsinki, Helsinki, Fi-00014, Finland
[3]Finnish Meteorological Institute, Helsinki, Fi-00101, Finland
[4]Institute of Environmental Physics, University of Bremen, Bremen, 28359, Germany

Correspondence to: Peng Lu (lupeng@dlut.edu.cn)

Abstract. Pond color, which creates the visual appearance of melt ponds on Arctic sea ice in summer, is quantitatively investigated using a two-stream radiative transfer model for ponded sea ice. The upwelling irradiance from the pond surface is determined, and then its spectrum is transformed into ~~the~~ RGB color space ~~through~~using a colorimetric method. The dependence of pond color on various factors such as water and ice properties and incident solar radiation is investigated. The results reveal that increasing underlying ice thickness H_i enhances both the green and blue components of pond color, whereas the red component is mostly sensitive to H_i for thin ice (H_i < 1.5 m) and to pond depth H_p for thick ice (H_i > 1.5 m), similar to the behavior of melt-pond albedo. The distribution of the incident solar spectrum F_0 with wavelength affects the pond color rather than its intensity. The pond color changes from dark blue to brighter blue with increasing scattering in ice, and the influence of absorption in ice on pond color is limited. The pond color reproduced by the model agrees well with field observations ~~on~~for Arctic sea ice in summer, which supports the validity of this study. More importantly, the pond color has been confirmed to contain information about meltwater and underlying ice, and therefore it can be used as an index to retrieve H_i and H_p. Retrievals of H_i for thin ice (H_i < 1 m) agree better with field measurements than retrievals for thick ice, but those of H_p are not good. The analysis of pond color is a new potential method to obtain thin ice thickness ~~information~~ in summer, although more validation data and improvements to the radiative transfer model will be needed in future.

1 Introduction

Melt ponds are the most distinctive characteristic of the Arctic sea ice surface during summer. They can cover up to 50% of the ice surface (Webster et al., 2015) and lower the surface albedo from ~~as high as~~ 0.8 (snow) to ~~as low as~~ 0.15 (pond) (Perovich and Polashenski, 2012). The albedo evolution generates a positive ice-albedo feedback mechanism, which enhances the melting of ice, alters the physical and optical properties of sea ice, and even affects the salt and heat budget of the ocean surface layer (Landy et al., 2015). As a result, melt ponds ~~are~~play an ~~issue as~~ important ~~and inevitable as~~role in the dramatic decay of current Arctic sea ice cover (Flocco et al., 2012).

Studies on melt ponds can be categorized with respect to three aspects: morphological observations, optical measurements, and modeling of the melting processes. Morphological studies focus on the distribution and physical properties of melt ponds using field observations and remote sensing (e.g. Huang et al., 2016). The melt-pond distribution determined by aerial photography was linked to the areally averaged surface albedo (Perovich et al., 2002b), and an obvious decrease in average surface albedo was discovered by comparing image-derived data with historical observations (Lu et al., 2010). A distinct variation trend in melt-pond fractions (MPF) in different regions of the Arctic Ocean has been found (Istomina et al, 2015) using MPF retrievals from satellite optical data (Rösel et al., 2012; Zege et al., 2015). Satellite passive microwave data were also employed to estimate MPF over high-concentration Arctic sea ice (Tanaka et al., 2016), serving as a basis for building time series of MPF in regions of consolidated ice pack. In-situ measurements of ice physics were carried out to demonstrate the mechanisms that enable melt-pond formation (Polashenski et al., 2012), and a newly found percolation blockage process was identified to be responsible for initial meltwater retention on highly porous first-year ice (FYI) (Polashenski et al., 2017).

Optical measurements focus mainly on the partition of solar radiation in melting sea ice (e.g. Nicolaus and Katlein, 2013). The melt-pond albedo has been found to vary with the melt stage of Arctic sea ice, and the seasonal evolution of ice albedo can be categorized into seven phases: cold snow, melting snow, pond formation, pond drainage, pond evolution, open water, and ~~freezeup~~freeze-up (Perovich and Polashenski, 2012). The transmittance through FYI was almost three times larger than through multiyear ice (MYI) according to measurements made using a remotely operated vehicle under summer sea ice. It resulted from the larger melt-pond coverage of FYI compared to MYI (Nicolaus et al., 2012). Ice thickness, scattering in ice, and melt-pond distribution were found to be primary factors dominating light transmission through ponded sea ice, although their impacts were different on small and large scales (Light et al., 2015; Katlein et al., 2015).

Finally, numerical simulations have been used to investigate the physical processes of melt ponds from formation to summertime development and then to autumn refreezing (e.g., Tsamados et al., 2015). A three-dimensional model was used to simulate the evolution of melt ponds and found that the role of snow is important mainly at the onset of melting, whereas initial ice topography strongly controls pond size and fraction throughout the melt season (Scott and Feltham, 2010). The refreezing process of melt ponds was also modeled, and the results revealed that ice growth would be overestimated by 26% if the impact of ~~trapped~~refrozen ponds was excluded (Flocco et al., 2015). New parameterizations for melt ponds have also been embedded into climate models to evaluate the role of surface melting on the summer decay of Arctic sea ice (e.g. Holland et al., 2012). The improved models produced results that agreed more closely with observations than other models without or only implicitly including the effect of melt ponds (Flocco et al., 2012; Hunke et al., 2013).

This study focuses on the color evolution of melt ponds on Arctic sea ice, a perspective on melt ponds that has seen few investigations so far (Perovich et al., 2002a; Light et al., 2015; Istomina et al., 2016). The photograph in Fig. 1 reveals the large variety in melt-pond appearances even on the same ice floe. The color of melt ponds varies from light bluish to dark, largely depending on the age of the pond and the properties of the underlying ice, which can be easily examined during field investigations. First quantitative measurements ~~on~~of melt-pond color have been performed in the ~~Central~~central Arctic in 2012 (Istomina et al., 2016). ~~Except for~~Beyond spectral albedo of sea ice and melt ponds measured with the portable radiometer ASD FieldSpecPro 3 (Istomina et al., 2013; Istomina et al., 2017), a photograph has been taken at each albedo measurement site, together with ice thickness and water depth measured by means of drilling. These field data show a clear connection between the underlying ice thickness of the melt pond and its color and spectral albedo. The effect of the water depth was found to be negligible. It has been suggested that the melt pond color can therefore be used for ice thickness estimates in summer (Istomina et al., 2016).

The motivation of this study is to elaborate on this idea and understand why the color of melt ponds can change and the micro-physical and optical reasons leading to such changes. Efforts ~~will~~are also ~~be~~ made to find ways to effectively use the information provided by pond color ~~more effectively because this color contains the optical response of melt ponds and sea ice to incident solar radiation~~. For example, information about sea-ice thickness below the melt pond, pond depth, and primary production in melt ponds could be retrieved.

To achieve these objectives, a radiative transfer model (RTM) initially developed to parameterize melt-pond albedo (Lu et al., 2016, hereafter LU16) is used. Section 2 introduces the color-retrieval method using the RTM. Section 3 investigates the influences of various factors, including pond depth, ice thickness, incident solar radiation, and inherent optical properties (IOPs), on melt-pond color. Section 4 discusses model uncertainty and retrievals from pond color, and Section 5 draws conclusions.

2 Methods

2.1 Radiative transfer model for melt pond

~~Albedo sensed by spectral radiometers represents the spectrum upwelling irradiance from the surface, but the~~The color of a melt pond is ~~actually~~ the response of human eyes to ~~this~~the upwelling irradiance from the surface, which consists of the reflected solar radiation from the pond surface and the backscattering radiation from ice and water below. Based on the spectral RTM for melt ponds in LU16, each part of the upwelling radiation can be determined, thus providing the necessary information to determine pond color.

For the two-layer model comprising of melt pond and underlying ice, radiation transfer is simplified as two streams, upwelling and downwelling irradiances. These are governed by two coupled first-order differential equations under the assumptions of diffuse incident solar radiation and isotropic scattering (Flocco et al., 2015). Assuming continuity of radiation fluxes at airpond, pond-ice, and ice-ocean interfaces, the irradiance in both directions in each layer can be calculated as well as the melt-pond albedo α_λ (see Eqs. (1–9) in LU16 for details).

2.2 Estimation of pond color from simulated upwelling spectrum

Along the whole solar spectrum, only the portion in the visible band, the wavelengths between λ_1 = 380 nm and λ_2 = 780 nm, is detectable by human eyes. To derive the color of an outgoing spectrum from the pond surface, $F_a(\lambda) = \alpha_\lambda F_0(\lambda)$ where $F_0(\lambda)$ is the incident solar irradiance, the two following methods are proposed.

The first is a mathematical method defining the color as the mean wavelength of the spectral distribution of light:

$$\bar{\lambda} = \frac{\int_{\lambda_2}^{\lambda_1} \lambda F_a(\lambda) d\lambda}{\int_{\lambda_2}^{\lambda_1} F_a(\lambda) d\lambda}, \quad (1)$$

where $\bar{\lambda}$ represents the 'mean color' of the melt pond. For example, $\bar{\lambda}$ = 475 nm denotes a blue color, 510 nm green, and 570 nm yellow.

The second approach is a colorimetric method based on the fact that human eyes with normal vision have three kinds of cone cells, which sense light with spectral sensitivity peaks at long (560–580 nm), middle (530–540 nm), and short (420–440 nm) wavelengths. International Commission on Illumination (CIE, 1986) defines three color matching functions, $\bar{x}(\lambda)$, $\bar{y}(\lambda)$, and $\bar{z}(\lambda)$, as numerical description of the chromatic response of a standard observer to an incident spectrum (Fig. 2a). Note that the peaks of color matching functions in Fig. 2a shift a little from those of cone cells above, and it is because modifications are necessary to avoid the mathematical difficulty as representing the color by negatives (Hunt, 2004). The tristimulus values in the XYZ color space for a reflective surface are given by:

$$\begin{cases} X = \frac{1}{N}\int_{\lambda_2}^{\lambda_1} \alpha_\lambda \cdot F_0(\lambda) \cdot \bar{x}(\lambda) d\lambda \\ Y = \frac{1}{N}\int_{\lambda_2}^{\lambda_1} \alpha_\lambda \cdot F_0(\lambda) \cdot \bar{y}(\lambda) d\lambda \\ Z = \frac{1}{N}\int_{\lambda_2}^{\lambda_1} \alpha_\lambda \cdot F_0(\lambda) \cdot \bar{z}(\lambda) d\lambda \\ \quad N = \int_{\lambda_2}^{\lambda_1} F_0(\lambda) \cdot \bar{y}(\lambda) d\lambda \end{cases}, \quad (2)$$

where Y is a measure of the perceived luminosity of the light and the X- and Z- components give the chromaticity of the spectrum. N is defined as the reference illuminant for the reflective surface~~, and the~~. The luminosity value (Y) is constrained in the range of 0–1.

The CIE XYZ color space can describe all colors visible to humans, but is not convenient for use in computer graphics or by a common output device such as an LED monitor. Therefore, the values in the XYZ space are converted into an RGB space, which specifies intensity values for red, green, and blue primary light to generate a desired color. This can be done by a linear transformation as:

$$\begin{bmatrix} r \\ g \\ b \end{bmatrix} = M^{-1} \begin{bmatrix} X \\ Y \\ Z \end{bmatrix} = \begin{bmatrix} X_r & X_g & X_b \\ Y_r & Y_g & Y_b \\ Z_r & Z_g & Z_b \end{bmatrix}^{-1} \begin{bmatrix} X \\ Y \\ Z \end{bmatrix}, \tag{3}$$

where r, g, and b are the intensities of red, green, and blue primaries that yield the desired color and M is the transformation matrix consisting of the coordinates of the three primaries in the XYZ space.

To obtain the matrix M, the CIE chromaticity diagram must be introduced (Fig. 2b), which describes a color in a two-dimensional chromaticity coordinate system (x, y) while ignoring its luminance Y. The XYZ ~~coordinates~~tristimulus values are thus scaled as:

$$\begin{cases} x = X/(X+Y+Z) \\ y = Y/(X+Y+Z) \\ z = Z/(X+Y+Z) \end{cases}. \tag{4}$$

These ~~coordinates~~values are dependent, $z = 1 - x - y$, and as illustrated in Fig. 2b this two-dimensional presentation can determine the given color (Hunt, 2004). For a given RGB space, the chromaticity coordinates are always given as the primary colors (x_r, y_r), (x_g, y_g), (x_b, y_b) and the white point (x_w, y_w).

According to Eq. (4), the transformation matrix M can be expanded as:

$$M = \begin{bmatrix} X_r & X_g & X_b \\ Y_r & Y_g & Y_b \\ Z_r & Z_g & Z_b \end{bmatrix} = \begin{bmatrix} (X_r+Y_r+Z_r)x_r & (X_g+Y_g+Z_g)x_g & (X_b+Y_b+Z_b)x_b \\ (X_r+Y_r+Z_r)y_r & (X_g+Y_g+Z_g)y_g & (X_b+Y_b+Z_b)y_b \\ (X_r+Y_r+Z_r)z_r & (X_g+Y_g+Z_g)z_g & (X_b+Y_b+Z_b)z_b \end{bmatrix}$$

$$= \begin{bmatrix} x_r & x_g & x_b \\ y_r & y_g & y_b \\ z_r & z_g & z_b \end{bmatrix} \begin{bmatrix} X_r+Y_r+Z_r & 0 & 0 \\ 0 & X_g+Y_g+Z_g & 0 \\ 0 & 0 & X_b+Y_b+Z_b \end{bmatrix} = A \cdot S, \tag{5}$$

where the matrix A is known from Fig. 2b. To obtain the unknown diagonal matrix S, the definition of the white point is used. The rgb intensities for the white point are $r = g = b = 1$. The luminosity is not specified in Fig. 2b; a full luminance can be used for the white point according to Eq. (2), that is, $Y_w = 1$. Substituting these values into Eq. (3):

$$\begin{bmatrix} X_w \\ Y_w \\ Z_w \end{bmatrix} = M \begin{bmatrix} 1 \\ 1 \\ 1 \end{bmatrix} \Rightarrow [X_w + Y_w + Z_w] \begin{bmatrix} x_w \\ y_w \\ z_w \end{bmatrix} = A \cdot S \cdot \begin{bmatrix} 1 \\ 1 \\ 1 \end{bmatrix}$$

$$\Rightarrow \frac{Y_w}{y_w}\begin{bmatrix} x_w \\ y_w \\ z_w \end{bmatrix} = A \cdot \begin{bmatrix} X_r + Y_r + Z_r \\ X_g + Y_g + Z_g \\ X_b + Y_b + Z_b \end{bmatrix} \Rightarrow \begin{bmatrix} X_r + Y_r + Z_r \\ X_g + Y_g + Z_g \\ X_b + Y_b + Z_b \end{bmatrix} = A^{-1} \cdot \begin{bmatrix} x_w/y_w \\ 1 \\ z_w/y_w \end{bmatrix}. \quad (6)$$

By combining Eqs. (5) and (6), the transformation matrix *M* is determined, and then the *rgb* intensities can be calculated using the *XYZ* ~~coordinates~~tristimulus values according to Eq. (3).

Comparing the two methods, the first one is straightforward, and the result is a mean wavelength corresponding to a monochromatic light, which is not particularly good to compare with human vision or to present by computer graphics according to Fig. 2b. The second method is complex, but gives the intensity of the three primaries, so that it provides a convenient way to reproduce color on a computer. The following analyses mainly focus on the results of the latter method.

3 Results

To calculate radiative transfer and color retrieval, certain parameters must to be specified. The IOPs of sea ice and water have been fully discussed in LU16, and the results are used here. The absorption coefficients of sea ice and water ($k_{\lambda,i}$, $k_{\lambda,w}$) are shown in Fig. 3. The former is a weighted average of contributions from pure ice and brine pockets, $k_{\lambda,i} = v_{pi}k_{\lambda,pi} + v_{bp}k_{\lambda,w}$ (Perovich, 1996) and varies within ±20% due to varying combinations of the volume fractions of pure ice v_{pi} and brine pockets v_{bp} (Huang et al., 2013). The mean curve of $k_{\lambda,i}$ in Fig. 3 is defined as the absorption coefficient of Arctic sea ice in summer. Note that $k_{\lambda,w}$ is lower than $k_{\lambda,pi}$ for λ < 560 nm, and higher than $k_{\lambda,pi}$ as λ > 560 nm. The weighted average $k_{\lambda,i}$ varies closer to $k_{\lambda,pi}$ than to $k_{\lambda,w}$ because of the large volume fraction of pure ice, but sometimes it is also lower than both $k_{\lambda,pi}$ and $k_{\lambda,w}$ especially for λ > 560 nm (Fig. 3). This happens only if there are lots of gas bubbles and little brine pockets contained in sea ice, and the absorption by gas bubbles is limited but their volume fraction cannot be neglected. Scattering in meltwater and ocean water is neglected ($\sigma_{\lambda,w} = 0$). The scattering coefficient of sea ice is independent of wavelength because the scattering inhomogeneities in ice are much larger than the wavelength of light. Perovich (1990) has investigated the values of scattering coefficient for different types of snow and ice. A value of σ_i = 2.5 m^{-1}, corresponding to white ice interior in Perovich (1990), has been promoted by LU16 for summer Arctic sea ice because it produces more comparable melt-pond albedo with field observations than others. The value is then employed in this study. The incident solar irradiance $F_0(\lambda)$ measured by Grenfell and Perovich (2008) under a completely overcast sky on August 7, 2005 with the solar disk not visible is used because it is representative of the Arctic summer, as in LU16. The chromaticity coordinates (*x*, *y*) of the primaries are (0.640, 0.330), (0.210, 0.710), and (0.150, 0.060) for red, green, and blue respectively and (0.313, 0.329) for the white point in the selected Adobe RGB color space (Adobe, 2005). These parameters are constant throughout the study unless otherwise defined.

The color of a melt pond changes with different factors such as sky conditions, ice properties, and pond depth (Light et al., 2015; Istomina et al., 2016). We investigate the influence of various factors on pond color in the following sections.

3.1 Influence of pond depth and ice thickness

~~According to experience and field observations, pond depth H_p and underlying ice thickness H_i are the two main factors influencing melt-pond albedo as well as color~~ In this study, we assumed H_p varies~~(Light et al., 2015; Istomina et al., 2016). Here, H_p is assumed to vary~~ between 0 and 0.5 m and H_i between 0.5 and 5.0 m. The range of ice thickness is somewhat beyond the current state in the Arctic summer (Lang et al., 2017). However, it is still beneficial to see the outcome of the proposed model at limiting conditions of thick deformed MYI. The results are shown in Fig. 4.

It is clear that the apparent optical properties of the melt pond are totally different for thin and thick ice. In Fig. 4a, the melt-pond albedo ~~is sensitive to~~depends mainly on H_i for thin ice~~, but to~~ (H_i < 1.5 m), and on H_p for thick ice~~,~~ (H_i > 1.5 m), as also illustrated by LU16. The mean wavelength of pond color as retrieved by Eq. (1) has similar features (Fig. 4b). However, the behavior of the three primary colors is somewhat different. The red component in Fig. 4c increases mostly with increasing H_i for thin ice (H_i < 1.5 m), but with increasing H_p for thick ice (H_i > 1.5 m), similarly to the wavelength-integrated albedo α_B in Fig. 4a. The green and blue components in Figs. 4d and 4e change only with H_i and almost not at all with H_p, except for very thick ice with H_i > 4 m. As a result, the simulated color of the melt pond made up of the RGB components, as shown in Fig. 4f, gradually changes from dark blue to bright blue with increasing underlying ice thickness. However, for thin ice of H_i < 1.5 m, the slight influence of H_p on pond color is also detectable. In other words, deeper pond water makes the color bluish rather than gray because red light is more easily absorbed by pond water. Basically, melt ponds on FYI in Arctic are shallow and flat, resulting in various gray color tones, while ~~MYI~~ melt ponds ~~are always deep~~on MYI may have relative larger depth ranges and ~~narrow~~more complex geometrical patterns, displaying green and blue (Polashenski et al., 2012; Webster et al., 2015). These agree well with the variations in Fig. 4f. The simulated pond color can be also compared with photographs during field investigations on Arctic sea ice in summer, such as in Fig. 1, which shows results that are visually close to Fig. 4f. Furthermore, the part with thinner underlying ice seems obviously darker than the rest (Fig. 1), agreeing with the trend revealed by Fig. 4f. More quantitative validations of pond color using field observations are presented in Section 3.5.

3.2 Influence of incident solar radiation level

Sky conditions of course affect the appearance of the ocean surface, but they are not considered here because of the assumption of diffuse incident radiation in the model. In this case, only the level of incident solar radiation, $F_0(\lambda)$, can be altered to investigate the influence on pond color. Except for the default value of $F_0(\lambda)$ on August 7 defined previously, five more irradiance spectra were selected according to Grenfell and Perovich (2008). All of them represent Arctic summer conditions under a completely overcast sky in August and September 2005 (Fig. 5a). In their work, the Arctic sky was never totally clear near the solar noon in August, but in September, cloud cover decreased somewhat, providing cloud-free periods. There is also a difference in the noon solar zenith angle between August and September at 70 °N–80 °N: it is 60 °–70 ° in August and 70 °–80 ° in September. These six cases differ widely with respect to $F_0(\lambda)$. Like LU16, H_p = 0.3 m and H_i = 1.0 m are used, corresponding to a clear water pond on typical Arctic FYI, and they are constant in following discussions unless otherwise defined. The results are shown in Fig. 5b.

It is surprising that the influence of $F_0(\lambda)$ on pond color is less pronounced than that of H_i and H_p in Fig. 4. The *rgb* intensities of pond color changed little under an overcast sky in August, so was the simulated color shown on the top of Fig. 5b. However, the results on overcast days in September, which produce a weaker red light but stronger blue light, show a brighter color than in August. $F_0(\lambda)$ was the only variable that could have caused the change. However, according to Fig. 5a, the incident spectra differed widely from each other and therefore were not the direct reason for the similar results in Fig. 5b.

If a normalized value of the incident irradiance is defined as $\omega = F_0(\lambda) / \int_{\lambda_2}^{\lambda_1} F_0(\lambda) d\lambda$, the difference is obvious according to Fig. 6. The level of F_0 on an overcast day decrease with date in Fig. 5a, and ω varies with obviously stronger energy in the shortwave band (< 530 nm), but less energy in the longwave band (> 530 nm). This trend becomes more pronounced with time according to Fig. 6. As a result, the color of the melt pond in September includes more contributions from blue light, but fewer from red light (Fig. 5b).

3.3 Influence of optical properties of ice

Optically active inclusions in sea ice, gas bubbles, brine pockets, and biota affect the appearance and color of melt ponds on summer Arctic sea ice (Kilias et al., 2014). However, the microstructure and physical properties of sea ice cannot be treated directly by our RTM. In this section, the scattering coefficient σ_i and the absorption coefficient $k_{\lambda,i}$, actually functions of the ice microstructure (Light et al., 2004), are investigated for their impact on pond color. The results are shown in Fig. 7.

The scattering coefficient of sea ice ranges from 1.2 to 2.5 m $^{-1}$, corresponding to sea ice ranging from melting blue ice with a small content of gas bubbles to porous white ice containing large quantities of gas bubbles according to Perovich (1990). The full range starting from $\sigma_i = 0$ is presented (Fig. 7a) to understand the model outcome for an idealized purely absorbing medium. Without scattering, the melt-pond albedo is 0.05, reflecting only specular reflectance at the air-water interface, and the *rgb* intensities of pond color are all at low level, producing a dark grey color. With σ_i increasing into a realistic range, both the albedo and the *rgb* intensities increase obviously, making the pond color brighter. Additionally, MYI in Arctic contains much less brine and more gas bubbles than FYI, then the more scattering in MYI is another possible factor causing the different color of melt ponds on MYI and FYI except for H_i and H_p (Fig. 4f).

For $k_{\lambda,i}$, the absorption coefficient of sea ice in Fig. 7b, the maximum and minimum values are determined from different combinations of volume fractions of pure ice and brine pockets (Fig. 4). With enhanced absorption in sea ice, the role of scattering in ice becomes less important, weakening the resulting upwelling irradiance, and the albedo and the *rgb* intensities consequently decrease. However, their changes are small compared with those shown in Fig. 7a, and the resulting variation in pond color is nearly undetectable.

The comparison in Fig. 7 clearly illustrates the importance of scattering in ice, which is the source of upwelling irradiance from the pond water and the ice interior. When scattering in ice is enhanced, the upwelling red, green and blue light from the pond surface will all be enhanced, with the red component enhanced less, producing a light blue pond color.

3.4 Variations during ice melt

It is interesting to see how the pond color develops during the process of ice melting. However, a complex thermodynamic model of sea ice would be needed to model in detail the changes in ice thickness and pond depth. For simplicity, an idealized model was used under the assumption of mass conservation, $H_i + \delta H_p = 1.3$ m, where δ is the ratio of water density ρ_w to ice density ρ_i, equal to 1.3 for porous ice in summer (Huang et al., 2013). Drainage of meltwater into the ocean and basal melt of sea ice were not considered to emphasize the influence of surface melting on pond color.

During sea-ice melting, as shown in Fig. 8, the ice thickness decreases from 1.3 m to 0, and the melt pond deepens from 0 to 1 m. At the same time, the pond albedo drops from 0.5 to 0.05, and the *rgb* intensities of pond color also decrease from about 0.6 to 0.05, resulting in an evolution of the pond color from gray to blue and then to almost black.

It is also noteworthy that variations in the red band are different from those in the green and blue bands. First, the red intensity is lower overall than that of the other bands during the melting process, which can be attributed to the fact that ice and water absorb red light more thoroughly than green and blue light (Fig. 3). Second, the red intensity drops nearly linearly along with ice melt, but the green and blue intensities drop faster at the end of ice melting than at the beginning. Red decreases linearly here because it is absorbed by the growing pond, whereas green and blue can maintain higher scattering because they can penetrate the pond almost to the end.

3.5 Comparisons with field observations

Validation of results is important, especially for the new method presented here, but most in-situ observations of pond color are visual and qualitative. The only quantitative measurements found for pond color were conducted by Istomina et al. (2016) on the Arctic sea-ice surface during the R/V Polarstern cruise ARK27/3 IceArc 2012. In addition to a portable spectroradiometer used for albedo measurements, a digital camera was used to take photographs of melt ponds, and the color information in the HSL (hue-saturation-luminance) color space was extracted to associate with concurrently measured pond depth and underlying ice thickness. The sky conditions were overcast during the optical measurements. Fog occurred frequently but its effect was limited, because the hand-held camera was close to the measured ponds and the work was stopped for heavy fog conditions. Additionally, some melt ponds observed by Istomina et al. (2016) were covered with a newly formed ice layer (1–3 cm). A new ice layer was then added to the RTM in section 2.1 to treat this situation, but the differences between an open pond and a refrozen pond were determined to be less than 3% in the primaries of the pond color. The influence of the transparent ice layer on pond reflection is therefore ignored.

Using the measured values for H_i and H_p, the pond color can be reproduced and compare with the in-situ observations (Fig. 9). Note that the *rgb* intensities calculated by the present model have been transformed into HSL values (0–1) to match the data in HSL color space reported by Istomina et al. (2016). The simulated pond color agrees well with the in-situ measurements by Istomina et al. (2016). The correlation coefficient is R = 0.822 with a significance level P < 0.01, the root-mean-square error is ε = 0.001, and the average of the relative error $<\xi>$ = 37%. The measured H_p was in the range of 8–40 cm and H_i in the range of 33–256 cm, producing varying pond color with a hue value in the 0.2–0.5 range, a saturation value within 0–0.5, and a luminance value within 0.4–0.6. The correspondingly simulated hue, saturation, and luminance values of pond color were within 0.4–0.5, 0–0.3, and 0.3–0.6 respectively. The agreement is acceptable because H_i and H_p are the only variables in the present model, but in-situ environmental conditions such as sky conditions and ice optics were different from pond to pond and of course not completely consistent with the definitions in the model. In other words, this experiment underlines the importance of H_i and H_p in determining the surface appearance of melt ponds (LU16) compared with other impact factors discussed above.

Obvious divergence can be found only at individual points. For examples, points a and b in Fig. 9 belong to the same melt pond with H_i = 0.33 m and H_p = 0.2 m, but the proposed model produced a relatively large difference in the hue and luminance values of pond color compared with other points. This pond is special because it has the thinnest underlying ice layer among all the measurements. It is suspected to be a mature melt pond that will melt through to the underlying ocean, in which case the brine channels in the underlying ice layer should be much larger and denser than in other cases, with different IOPs from the present model. Point c belongs to another melt pond that has the largest saturation value among all measurements of pond color, but the proposed model reproduced a lower value.

H_i and H_p are changing variables in the calculation. Uncertainties, among others, are the different in-situ conditions, such as sky conditions and ice optical properties, which need to be specified in the model since these in-situ properties were not measured in Istomina et al. (2016). We therefore carried out sensitivity studies by altering the values of F_0, σ_i, and $k_{\lambda,i}$ within reasonable ranges for Arctic sea ice in summer to reveal their impacts on the simulated pond color. The negative error bars in the simulated values in Fig.9 are associated with the scattering in ice as σ_i drops from the default value (2.5 m^{-1}) to 1.2 m^{-1} (Fig. 7a). The positive error bars are induced by F_0 as it decreases from the representative data in August to low levels in September (Fig. 5a). The influence of ice absorption coefficient on the simulated pond color is very limited (< 0.02), similar with Fig. 5b, and therefore not included in the error bars. It is revealed on Fig.9 that the impact of σ_i on the hue and saturation values is less than 0.05, and that on the luminance is less than 0.14. On the contrary, variation in the luminance value due to

F_0 is less than 0.04, and that in the hue and saturation is less than 0.15. That is, the maximum uncertainty in the simulated hue, saturation, and luminance values will not exceed 0.2 for different combinations of incident solar radiation and IOPs for summer sea ice. More importantly, these variations still locate almost within the range of $\pm 2\varepsilon$, namely the 95% confidence interval (Fig. 9). In other words, this experiment underlines the importance of H_i and H_p in determining the color of melt ponds compared with other impact factors.

4 Discussions

4.1 Uncertainties in pond-color estimation

Color is a highly subjective parameter associated with human visual perception, and therefore different people will have different descriptions even of the exact same color. Although colorimetry has provided tools to quantify and describe physically human color perception, it is still difficult to reproduce accurately the color of a reflecting surface (Fig. 9). This is true especially in the Arctic Ocean, with its severe weather conditions. Therefore, it is important to understand the limitations and uncertainties of the present method.

The first question arises from the assumption of the RTM in Section 2.1, in which diffuse incident radiation is assumed and scattering must be taken as isotropic. The former assumption is not a major problem in the summer Arctic due to the frequent presence of low stratus cloud cover. The latter assumption may, however, be inappropriate for sea ice, which possibly has more forward scattering than backward scattering, but actually most studies have still treated scattering in sea ice as isotropic (Katlein et al., 2014). Moreover, internal melting makes sea ice more porous in summer, and as a result the geometric structure of ice becomes more irregular, which can favor isotropic scattering (e.g., Leppäranta et al., 2003). Consequently, one may expect that the assumption of isotropic scattering is not much biased for melting sea ice. ~~Besides, it~~It is also assumed here that melt pond water is clean and scattering can be neglected (LU16). This is true if the water is meltwater from snow, and is also acceptable for ice meltwater or percolated Arctic sea water. There are no observations of any optically active impurities in melt ponds to the authors' knowledge, and the approximation has been shown valid for melt ponds shallower than 1 m (Podgorny and Grenfell, 1996). Dirty ponds with a sediment-covered floor or with cryoconite holes as observed by Eicken et al. (1994) are not considered here, and frozen melt ponds with a snow or thick ice cover in autumn (Flocco et al., 2015) are also excluded from this study.

The second question arises from the definition of the colorimetric method as retrieving the RGB components from a spectrum. Three color matching functions $\bar{x}(\lambda)$, $\bar{y}(\lambda)$, and $\bar{z}(\lambda)$, are used in Eq. (2) to quantify the chromatic response of the observer. These functions have been determined through a series of experiments that aimed to judge colors while looking through a hole with a 2° field of view (Wright, 1928; Guild, 1931). By 1960s, new color matching functions corresponding to a 10° standard observer were developed (Stiles and Birch, 1959). The 10° observer is currently believed to provide the best representation of the average spectral response of human observers, although the 2° observer still has its place for measuring objects that will be viewed at a distance. In addition, various RGB color spaces such as sRGB, Apple RGB, and Adobe RGB have been defined to satisfy the display of colors on different kinds of output devices (Süsstrunk et al., 1999), and they have different chromaticity coordinates for red, green, blue, and white colors in Fig. 3b. Tests have revealed that the differences between the two functions and among various RGB color spaces are not large enough to produce significantly different pond colors in this study, and therefore these results are not presented here.

The third question is associated with field observations of the color of melt ponds. Digital cameras used during field observations always have a viewing angle different from the standard observer defined previously, thus producing a different response to the incident spectrum. Besides, the color on photographs highly depends on the camera and the photographic parameters such as ISO and aperture values (Istomina et al., 2016), also making the direct comparisons of pond color between simulated results and field measurements difficult. Istomina et al. (2016) used RAW photographic data, which can save much more information about the light field during field observations than common image formats such as JPG, to calculate pond color. In addition, the incident solar radiation reaching the ice surface changes continuously in the Arctic Ocean, but for simplification, a constant F_0 was used in this study as a representative condition of the Arctic summer. However, the results shown in Fig. 5 illustrate that the influence of F_0 is not as important as the contributions from other impact factors.

4.2 Possibility of retrieving pond depth and ice thickness

Like melt-pond albedo, pond color is also affected by many factors. Among them, pond depth and underlying ice thickness are the most important according to earlier discussions. Pond color can therefore be expressed by a function such as $C = f(H_i, H_p)$ if other impact factors discussed in Section 3 are treated as empirical constants. This implies a possibility of using pond color to retrieve H_i and H_p through solving the inverse problem, namely $(H_i, H_p) = f^{-1}(C)$. Since pond water is purely absorbing and ice is strongly scattering, the inverse function is well-defined., i.e. there exists a unique solution.

The incident solar spectrum covers the wavelength from 300 nm to 3000 nm (Grenfell and Perovich, 2008), but most of the long waves are absorbed in the first few centimetres of water or ice because the absorption coefficients in the longwave band are larger than those in the shortwave band by at least two orders of magnitude (Warren, 1984). This means that the upwelling irradiance resulting from scattering in ice mainly consists of visible light. The color of melt ponds, which is produced by upwelling irradiance, is actually the response of the whole mass of pond water and its underlying ice regime to the incident solar spectrum, thus providing a theoretical possibility of retrieving the properties of pond water and its underlying ice from the apparent pond color.

On the other hand, the relationship between pond color and meltwater depth or sea-ice thickness has actually been qualitatively determined by many field investigations (e.g., Perovich et al., 2002a). Istomina et al. (2016) found that the underlying ice thickness has a strong impact on the saturation value of pond color, but that the effect of pond depth is small. Variations in hue and luminance values of pond color are limited and a relation to either H_i or H_p could not be observed. These results provided a quantitative validation of the relationship proposed here and also proved the possibility of ice property retrieval from pond color. The camera dependency of the relationship was highlighted and RAW format imagery was suggested to decrease this dependency.

Both RGB and HSL color spaces have been used in this study. Basically, they are just different mathematical descriptions of color, and there are no notable differences between them. The conversion between them is also simple. The HSL color space is used to match the measurements by Istomina et al. (2016) and to examine the inverse problem $(H_i, H_p) = f^{-1}(H, S, L)$. A least-squares method is used, and the error function is defined as the Euclidean distance between the measured and simulated pond color in the HSL color space:

$$\Delta = |(H,S,L)_{\mathrm{SIM}} - (H,S,L)_{\mathrm{MEA}}| = \sqrt{c_H \cdot (H_{\mathrm{SIM}} - H_{\mathrm{MEA}})^2 + c_s \cdot (S_{\mathrm{SIM}} - S_{\mathrm{MEA}})^2 + c_L \cdot (L_{\mathrm{SIM}} - L_{\mathrm{MEA}})^2}\,, \quad (7)$$

where the subscript SIM denotes simulated results and MEA denotes *in-situ* measurements. The parameters c_H, c_S, and c_L indicate the different sensitivity of hue, saturation, and luminance values of pond color on pond depth and ice thickness, and they are determined by normalizing the square of correlation coefficient R^2 between the HSL values and the measured H_i and H_p. According to the statistical analyses in Istomina et al. (2016), there is $c_H = 0.255$, $c_S = 0.712$, and $c_L = 0.033$ (Table 1). Then an ergodic procedure using different combinations of H_i and H_p within reasonable ranges, 0–3 m for H_i and 0–0.5 m for H_p, can be performed to produce the minimum Δ, from which the estimated H_i and H_p can finally be determined. The retrievals of H_i and H_p using measured pond color by Istomina et al. (2016) and comparisons with field measurements are shown in Fig. 10.

A clear relationship between simulated and measured pond depth is not apparent in Fig. 10a, implying that the association of H_p with melt-pond color may be somewhat loose. This result agrees with Istomina et al. (2016). The relationship between simulated and measured ice thickness is also not clear, but a good agreement can be found for thin ice with $H_i < 1$ m (Fig. 10b). This means, first, that the underlying ice thickness rather than the pond depth can be easily obtained from pond color, and second, that the present retrieval method is more suitable for thin ice than for thick ice.

The first statement can be partly explained by Fig. 4, which shows that the dependence of pond color on ice thickness is obviously stronger than that on pond depth except for thick ice, $H_i > 1.5$ m in Fig. 4c. Moreover, the upwelling irradiance comes mainly from scattering in ice, and therefore the pond color is associated more with the underlying ice than with the pond water. The second statement is associated with the assumptions in the present RTM, which treats the pond water and underlying ice as parallel layers with uniform IOPs. This assumption is more valid for thin FYI because FYI typically has larger, but shallower, ponds than MYI due to the rougher topography of MYI in general (Webster et al., 2015). Hence, measurements on MYI are more affected by the contrasts at the boundary between ponded and bare ice (Taskjelle et al., 2017), which depart from the definition of the RTM. Another possible explanation comes from ice thickness since thin ice passes through more light than thick ice. With dark ocean beneath, the thinner domain shows a better discrimination as light at some wavelengths simply does not get backscattered, and that wavelength cutoff varies quickly with ice thickness.

Nevertheless, the result shown in Fig. 10b is still encouraging. The squared correlation coefficient between simulated and measured ice thickness is R^2R = 0.671819, and the correlation is significant (P = 0.02). The root-mean-square error is ε = 0.156 m. The relative error ξ, defined as the ratio of the absolute difference to the measured value, presents an average of 29% and a maximum of 50%. The resultAlthough the correlation coefficient for the subset of H_i < 1 m in Fig. 10b is acceptablenot highly increased as comparing with that in Fig. 10a, because of the very few available data herepoints in the subset, the improvements in the errors of retrievals are significant. The values of ε and $<\xi>$ in Fig. 10b are approximately 1/3 and 1/2, respectively, of those in Fig. 10a. More validations from field observations are likely to improve the retrieve model in Eq. (7) and then further reduce the error in retrievals.

The results give support for a possible new method of determining the sea-ice thickness, especially for meltingthin sea ice. This new method willwould complement our knowledge about sea ice thickness since presently most sea-ice thickness retrievals from satellite remote sensing are not good during the Arctic summer because of surface melt on ice (Kwok, 2010). The limitations and applicability of the color-retrieval method are clear from the previous discussions. First, this method is valid for thin ice with thickness less than 1 m, and when the melt ponds on top of ice are open or just covered by very thin ice. Frozen melt ponds with a snow or thick ice cover, having an obviously different appearance from open ponds, are excluded from this method. Second, overcast sky conditions are preferable for this method. They are prevailing although not always present during summer in Arctic. However, further work is still needed to cover clear sky conditions. Finally, satellite remote sensing has been employed to determine MPF (e.g. Istomina et al., 2015), but it is still difficult for the satellite instruments to detect melt-pond color because of the small spatial scale of melt ponds. In contrast, hand-held photography (e.g. Istomina et al., 2016), ship-borne photography (e.g. Lu and Li, 2010), and airborne photography (e.g. Lu et al., 2010) are very effective ways to get the small-scale information on ice surface and provide a basis for ice thickness retrievals. Especially, with unmanned aerial vehicles (UAVs) equipped with a digital camera it is easy to observe sea ice surface features, including melt-pond color, at a floe scale, which has been successfully tested during the 7th Chinese Arctic cruise in 2016 (Wang et al., 2017).

5 Conclusions

A two-stream radiative transfer model was adopted and applied to ponded Arctic sea ice to examine the upwelling irradiance from the pond surface. A colorimetric method was provided to transform the upwelling spectrum into a color in the RGB color space, providing a way for comparisons with human vision and computer graphics. The dependence of pond color on the properties of the pond water and underlying sea ice was quantitatively and thoroughly investigated, and the use of pond color to retrieve the properties of ponded sea ice was also discussed.

The results reveal that both pond depth H_p and underlying ice thickness H_i have an important impact on pond color (Fig. 4). The green and blue intensities increase only with increasing H_i except for very thick ice with $H_i > 4$ m, but the red intensity increases mostly with increasing H_i for thin ice ($H_i < 1.5$ m) and with increasing H_p for thick ice ($H_i > 1.5$ m), similarly to melt-pond albedo (LU16). The reproduced pond color gradually changes from dark blue to bright blue with increasing H_i, visually agreeing with in-situ photography of melt ponds in the Arctic summer.

The influence of the level of incident solar irradiance, F_0, is limited, but its spectral distribution can cause detectable variations in pond color. The incident solar spectrum has lower radiative energy in September than in August, but it is more concentrated at short wavelengths (< 530 nm) than at long wavelengths (> 530 nm) (Figs. 5 and 6). Then the red intensity decreases, whereas the blue intensity increases as F_0 changes from August to September.

The IOPs of meltwater and sea ice are prescribed in the present model. In nature, the optical properties of water are more stable than those of sea ice, which change with the microstructure of ice during melting (Light et al., 2004). A sensitivity study reveals that the influence of variations in sea-ice absorption coefficient is limited, but that scattering plays an important role in pond color (Fig. 7). With increasing scattering in ice, all *rgb* intensities clearly increase, making the blue pond color brighter.

In a simplified melt case with $H_i + \delta H_p = 1.3$ m, where $\delta = 1.3$ the ratio of water and ice density, all *rgb* intensities of pond color decrease significantly from about 0.6 to 0.05, with the resulting color varying from gray to blue and then to black. The variation in red intensity is slightly different from those of green and blue: it is lower in value, and it drops linearly with ice melt, in contrast to the nonlinear decline of the other two primary colors (Fig. 8). In a real melt process, phase transition exists not only at ice surface but also in ice interior. If H_i and H_p are calculated by a thermodynamic model (e.g. Tsamados et al., 2015), and IOPs of sea ice are associated with ice physical parameters (e.g. Light et al., 2004), for example, ice porosity, then the seasonal evolutions in the color and albedo of melt ponds can be determined straightforwardly. However, it is out of the scope of the present paper and can be investigated in further studies.

The pond colors produced by the present model agree well with the pond-color measurements in the HSL color space reported by Istomina et al. (2016), proving the veracity of the proposed model and also implying the possibility of retrieving pond depth and ice thickness information from pond color (Fig. 9). A least-squares method was used to determine these quantities from three color components HSL. The results reveal a better agreement for ice thickness than for pond depth, and that the present model provides better retrieval for thin FYI than for thick MYI. The former is attributed to be obviously higher dependence of pond color on ice thickness than on pond depth (Fig. 4). The latter is partly because that the plane-parallel assumption agrees more closely with ponds on flat sea ice than on rough ice, and also possibly due to the higher transparency of thin ice than thick ice.

As the first quantitative study on the color of melt ponds, this study investigated not only the extent to which pond color depends on various factors, such as H_i, H_p, F_0, and IOPs, but also illustrated a potential method to use pond-color data to obtain ice thickness. Many ways have been developed to obtain information on sea-ice thickness using remote-sensing technologies and drilling (Wadhams, 2005; Leppäranta, 2011), but none of them is easy and cheap to conduct in the Arctic, and most are not feasible under summer conditions. In comparison, retrieval of ice thickness from pond color has an obvious advantage over all other methods because hand. Hand-held, ship-borne or airborne photography of melt ponds, especially widespread UAVs equipped with a digital camera, is easy to perform during field campaigns, although the color-retrieval method is constrained by preconditions such as open melt ponds, thin ice, and overcast sky.. A recent publication by Malinka et al. (2017) suggested another way to determine pond depth and ice thickness from measured spectral albedo of melt ponds. They obtained better retrievals of H_i and H_p partly because they used more complicated spectra as input compared with our case. As the first insight into the color of melt ponds, we tend to pose a The possibility instead of draw a conclusion because ofof a color-retrieval method was explored in this study using the limited available observations so far. The authors believe that more useful information can be extracted from the color of melt ponds if further in-situ validation data can be obtained and if the RTM can be improved to suit different ice types and sky conditions.

Acknowledgements. This research was supported by the Global Change Research Programme of China (2015CB953901), the National Natural Science Foundation of China (41676187 and 41376186). M.L. was supported by the EU FP7 Project EuRuCAS (European-Russian Centre for Cooperation in the Arctic and Sub-Arctic Environmental and Climate Research, Grant no. 295068) and the Academy of Finland (11409391), and B.C. was supported by the NSFC research facility mobility (41428603) and the Academy of Finland (283101). L.I. and G.H. conducted the study in the framework of the project: Spaceborne observations for detecting and forecasting sea ice cover extremes (SPICES) funded by the European Union (H2020) (Grant no. 640161). The authors are grateful to the scientific party of the ARK 27/3 cruise for making the sea ice optical measurements possible. Special thanks are expressed to Marcel Nicolaus for organizing the logistics and to the Sea Ice Physics group on board for assisting with the measurements. Three anonymous reviewers and the editor Jennifer Hutchings are also acknowledged for their constructive comments to highly improve the manuscript.

References

Adobe AGB (1998): Color image encoding. Availabe at www.Adobe.com, San Jose, USA, 2005.

Commission Internationale de l'Éclairage (CIE): Standard on colorimetric observers, CIE S002, 1986.

Eicken, H., Alexandrov, V., Gradinger, R., Ilyin, G., Ivanov, B., Luchetta, A., Martin, T., Olsson, K., Reimnitz, E., Pac, R., Poniz, P. and Weissenberger, J.: Distribution, structure and hydrography of surface melt puddles, Ber. Polarforsch, 149, 73–76, 1994.

Flocco, D., Feltham, D. L., Bailey, E. and Schroeder, D.: The refreezing of melt ponds on Arctic sea ice, J. Geophys. Res. Oceans, 120, 647–659, doi:10.1002/2014JC010140, 2015.

Flocco, D., Schroeder, D., Feltham, D. L. and Hunke, E. C.: Impact of melt ponds on Arctic sea ice simulations from 1990 to 2007, J. Geophys. Res., 117, C09032, doi:10.1029/2012JC008195, 2012.

Grenfell, T. C. and Perovich, D. K.: Radiation absorption coefficients of polycrystalline ice from 400–1400 nm, J. Geophys. Res., 86, 7447–7450, 1981.

Grenfell, T. C. and Perovich, D. K.: Incident spectral irradiance in the Arctic Basin during the summer and fall, J. Geophys. Res., 113, D12117, doi:10.1029/2007JD009418, 2008.

Guild, J.: The colorimetric properties of the spectrum, Phil. Trans. R. Soc. A, 230, 149–187, 1931.

Holland, M. M., Bailey, D. A., Briegleb, B. P., Light, B. and Hunke, E.C.: Improved sea ice shortwave radiation physics in CCSM4: the impact of melt ponds and aerosols on arctic sea ice, J. Clim., 25, 1413–1430, 2012.

Huang, W., Lei, R., Ilkka, M., Li, Q., Wang, Y. and Li, Z.: The physical structures of snow and sea ice in the Arctic section of 150 °–180 °W during the summer of 2010, Acta Oceanol. Sin., 32, 57–67, doi:10.1007/s13131-013-0314-4, 2013.

Huang, W., Lu, P., Lei, R., Xie, H. and Li, Z.: Melt pond distribution and geometry in high Arctic sea ice derived from aerial investigations, Ann. Glaciol., 57, doi:10.1017/aog.2016.30, 2016.

Hunke, E. C., Hebert, D. A. and Lecomte, O.: Level-ice melt ponds in the Los Alamos sea ice model, CICE, Ocean Model., 71, 26–42, 2013.

Hunt, R. G. W.: The reproduction of colour, 6th ed. John Wiley & Sons, pp. 844, 2004.

Istomina, L., Heygster, G., Huntemann, M., Marks, H., Melsheimer, C., Zege, E., Malinka, A., Prikhach, A. and Katsev, I.: Melt pond fraction and spectral sea ice albedo retrieval from MERIS data – Part 2: Case studies and trends of sea ice albedo and melt ponds in the Arctic for years 2002–2011, The Cryosphere, 9, 1567–1578, doi:10.5194/tc-9-1567-2015, 2015.

Istomina, L., Melsheimer, C., Huntemann, M., Nicolaus, M. and Heygster, G.: Retrieval of sea ice thickness during melt season from in situ, airborne and satellite imagery, IEEE International Geoscience and Remote Sensing Symposium (IGARSS), Beijing, 7678–7681, doi: 10.1109/IGARSS.2016.7731002, 2016.

Istomina, L., Nicolaus, M. and Perovich, D. K.: Spectral albedo of sea ice and melt ponds measured during POLARSTERN cruise ARK-XXVII/3 (IceArc) in 2012, Institut für Umweltphysik, Universität Bremen, doi:10.1594/PANGAEA.815111, 2013.

Istomina, L., Nicolaus, M. and Perovich, D. K.: Spectral albedo, water depth and ice thickness within melt ponds measured during POLARSTERN cruise ARK-XXVII/3 (IceArc) in 2012, Dataset #876210, DOI registration in progress, 2017.

Katlein, C., et al.: Influence of ice thickness and surface properties on light transmission through Arctic sea ice, J. Geophys. Res. Oceans, 120, doi:10.1002/2015JC010914, 2015.

Katlein, C., Nicolaus, M. and Petrich, C.: The anisotropic scattering coefficient of sea ice, J. Geophys. Res. Oceans, 119, doi:10.1002/2013JC009502, 2014.

Kilias, E. S., Peeken, I. and Metfies, K.: Insight into protist diversity in Arctic sea ice and melt-pond aggregate obtained by pyrosequencing, Polar Res., 33, 23466, doi:10.3402/polar.v33.23466, 2014.

Kwok, R.: Satellite remote sensing of sea-ice thickness and kinematics: a review, J. Glaciol., 56, 1129–1140, 2010.

Landy, J. C., Ehn, J. K. and Barber, D. G.: Albedo feedback enhanced by smoother Arctic sea ice, Geophys. Res. Lett., 42, doi:10.1002/2015GL066712, 2015.

Lang, A., Yang, S. and Kaas, E.: Sea ice thickness and recent Arctic warming, Geophys. Res. Lett., 44, 409–418, doi:10.1002/2016GL071274, 2017.

Leppäramta, M.: The drift of sea ice, 2nd ed. Springer-Praxis, Heidelberg, Germany, 2011.

Leppäranta, M., Reinart, A., Arst, H., Erm, A., Sipelgas, L. and Hussainov, M.: Investigation of ice and water properties and under-ice light fields in fresh and brackishwater bodies, Nord. Hydrol., 34, 245–266, 2003.

Light, B., Maykut, G. A. and Grenfell, T.C.: A temperature-dependent, structural-optical model of first-year sea ice, J. Geophys. Res., 109, C06013, doi:10.1029/2003JC002164, 2004.

Light, B., Perovich, D. K., Webster, M. A., Polashenski, C. and Dadic, R.: Optical properties of melting first-year Arctic sea ice, J. Geophys. Res. Oceans, 120, doi:10.1002/2015JC011163, 2015.

Lu, P., Leppäranta, M., Cheng, B. and Li, Z.: Influence of melt-pond depth and ice thickness on Arctic sea-ice albedo and light transmittance, Cold Reg. Sci. Technol., 124, 1–10, doi:10.1016/j.coldregions.2015.12.010, 2016.

Lu, P., and Li, Z.: A method of obtaining ice concentration and floe size from shipboard oblique sea ice images. IEEE T. Geosci. Remote Sens., 48(7), 2771-2780, 2010.

Lu, P., Li, Z., Cheng, B., Lei, R. and Zhang, R.: Sea ice surface features in Arctic summer 2008: aerial observations, Remote Sens. Environ., 114(4): 693–699, 2010.

Malinka, A., Zege, E., Istomina, L., Heygster, G., Spreen, G., Perovich, D., and Polashenski, C.: Reflective properties of melt ponds on sea ice, The Cryosphere Discuss., https://doi.org/10.5194/tc-2017-150, in review, 2017.

Nicolaus, M. and Katlein, C.: Mapping radiation transfer through sea ice using a remotely operated vehicle (ROV), The Cryosphere, 7, 763–777, doi:10.5194/tc-7-763-2013, 2013.

Nicolaus, M., Katlein, C., Maslanik, J. and Hendricks, S.: Changes in Arctic sea ice result in increasing light transmittance and absorption, Geophys. Res. Lett., 39, L24501, doi:10.1029/2012GL053738, 2012.

Perovich, D. K.: Theoretical estimates of light reflection and transmission by spatially complex and temporally varying sea ice covers, J. Geophys. Res. 95, 9557–9567, doi:10.1029/JC095iC06p09557, 1990.

Perovich, D. K.: The optical properties of sea-ice. Cold Reg. Res. and Eng. Lab. (CRREL) Report 96-1, 585 Hanover, NH, 1996

Perovich, D. K., Grenfell, T. C., Light, B. and Hobbs, P. V.: Seasonal evolution of the albedo of multiyear Arctic sea ice, J. Geophys. Res., 107, doi:10.1029/2000JC000438, 2002a.

Perovich, D. K., Tucker III, W. B. and Ligett, K. A.: Aerial observations of the evolution of ice surface conditions during summer, J. Geophys. Res., 107, doi:10.1029/2000JC000449, 2002b.

Perovich, D. K. and Polashenski, C.: Albedo evolution of seasonal Arctic sea ice, Geophys. Res. Lett., 39, L08501, doi:10.1029/2012GL051432, 2012.

Podgorny, I. A. and Grenfell, T. C.: Partitioning of solar energy in melt ponds from measurements of pond albedo and depth, J. Geophys. Res., 101(C10), 22737–22748, 1996.

Polashenski, C., Golden, K. M., Perovich, D. K., Skyllingstad, E., Arnsten, A., Stwertka, C. and Wright, N.: Percolation blockage: A process that enables melt pond formation on first year Arctic sea ice, J. Geophys. Res. Oceans, 122, doi:10.1002/2016JC011994, 2017.

Polashenski, C., Perovich, D. and Courville, Z.: The mechanisms of sea ice melt pond formation and evolution, J. Geophys. Res., 117, C01001, doi:10.1029/2011JC007231, 2012.

Rösel, A., Kaleschke, L. and Birnbaum, G.: Melt ponds on Arctic sea ice determined from MODIS satellite data using an artificial neural network, The Cryosphere, 6, 431–446, doi:10.5194/tc-6-431-2012, 2012.

Scott, F. and Feltham, D. L.: A model of the three-dimensional evolution of Arctic melt ponds on first-year and multiyear sea ice, J. Geophys. Res., 115, C12064, doi:10.1029/2010JC006156, 2010.

Smith, R. C. and Baker, K. S.: Optical properties of the clearest natural waters (200–800 nm), Appl. Optics, 20, 177–184, 1981.

Stiles, W. S. and Birch, J. M.: N.P.L. Colour-matching investigation: Final report (1958), Optica Acta., 6, 1–26, doi:10.1080/713826267, 1959.

Süsstrunk, S., Buckley, R. and Swen, S.: Standard RGB color spaces, Color and Imaging Conference, 7, 127–134, 1999.

Tanaka, Y., Tateyama, K., Kameda, T. and Hutchings, J. K.: Estimation of melt pond fraction over high concentration Arctic sea ice using AMSR-E passive microwave data, J. Geophys. Res. Oceans, 121, doi:10.1002/2016JC011876, 2016.

Taskjelle, T., Hudson, S. R., Granskog, M. A. and Hamre, B.: Modelling radiative transfer through ponded first-year Arctic sea ice with a plane parallel model, The Cryosphere Discuss., doi:10.5194/tc-2017-36, in review, 2017.

Tsamados, M., Feltham, D., Petty, A., Schroeder, D. and Flocco, D.: Processes controlling surface, bottom and lateral melt of Arctic sea ice in a state of the art sea ice model, Phil. Trans. R. Soc. A, 373, 20140167, doi:/10.1098/rsta.2014.0167, 2015.

Wadhams, P.: Arctic sea ice thickness-A review of current technique and future possibilities, Proceedings of International Workshop on Arctic Sea Ice Thickness: past, present, and future, Denmark, 12–23, 2005.

Warren, S. G.: Optical constants of ice from the ultraviolet to the microwave, Appl. Optics, 23, 1206-1225, 1984.

Wang, M., Su, J., Li, T., Wang, X., Ji, Q., Cao, Y., Lin, L., Liu, Y.: Study on the method of extracting Arctic melt pond and roughness information on sea ice surface based on UAV observation, Chinese J. Polar Res., 29(4), 436–445, 2017. (In Chinese)

Webster, M. A., Rigor, I. G., Perovich, D. K., Richter-Menge, J. A., Polashenski, C. M. and Light, B.: Seasonal evolution of melt ponds on Arctic sea ice, J. Geophys. Res. Oceans, 120, doi:10.1002/2015JC011030, 2015.

Wright, W. D.: A re-determination of the trichromatic coefficients of the spectral colours, Trans. Opt. Soc., 30, 141–164, 1928.

Zege, E., Malinka, A., Katsev, I., Prikhach, A., Heygster, G., Istomina, L., Birnbaum, G. and Schwarz, P.: Algorithm to retrieve the melt pond fraction and the spectral albedo of Arctic summer ice from satellite optical data, Remote Sens. Environ., 163, 153–164, 2015.

Table 1: The squared correlation coefficients R^2 between melt-pond color and H_i and H_p in Istomina et al. (2016), and the deduced coefficients c_H, c_S, and c_L for Eq. (7).

Parameter	Coefficient	R^2		
		Total	H_i	H_p
Hue	0.255 (c_H)	0.301	0.266	0.035
Saturation	0.712 (c_S)	0.842	0.759	0.083
Luminosity	0.033 (c_L)	0.039	0.020	0.019

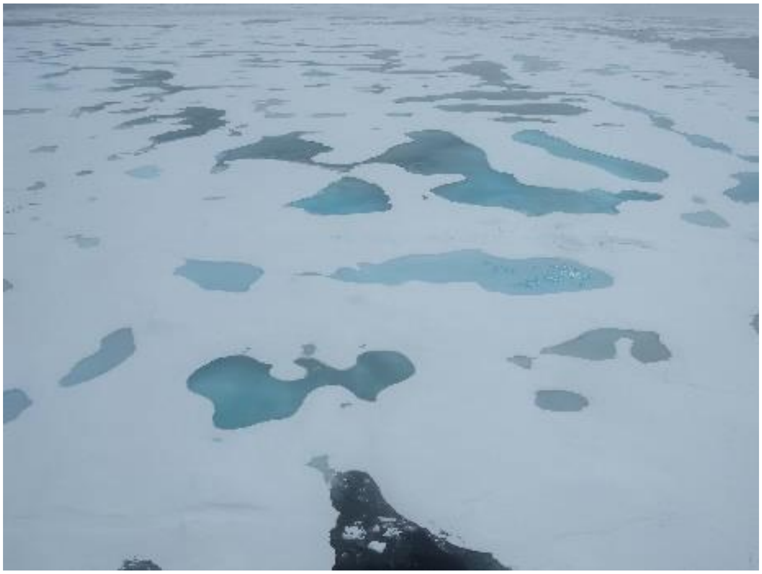

Figure 1: A typical image of melt ponds on Arctic sea ice captured onboard R/V *Xuelong* during the Chinese National Arctic Research Expeditions in summer 2016, clearly illustrating the large variability of pond color even on the same ice floe.

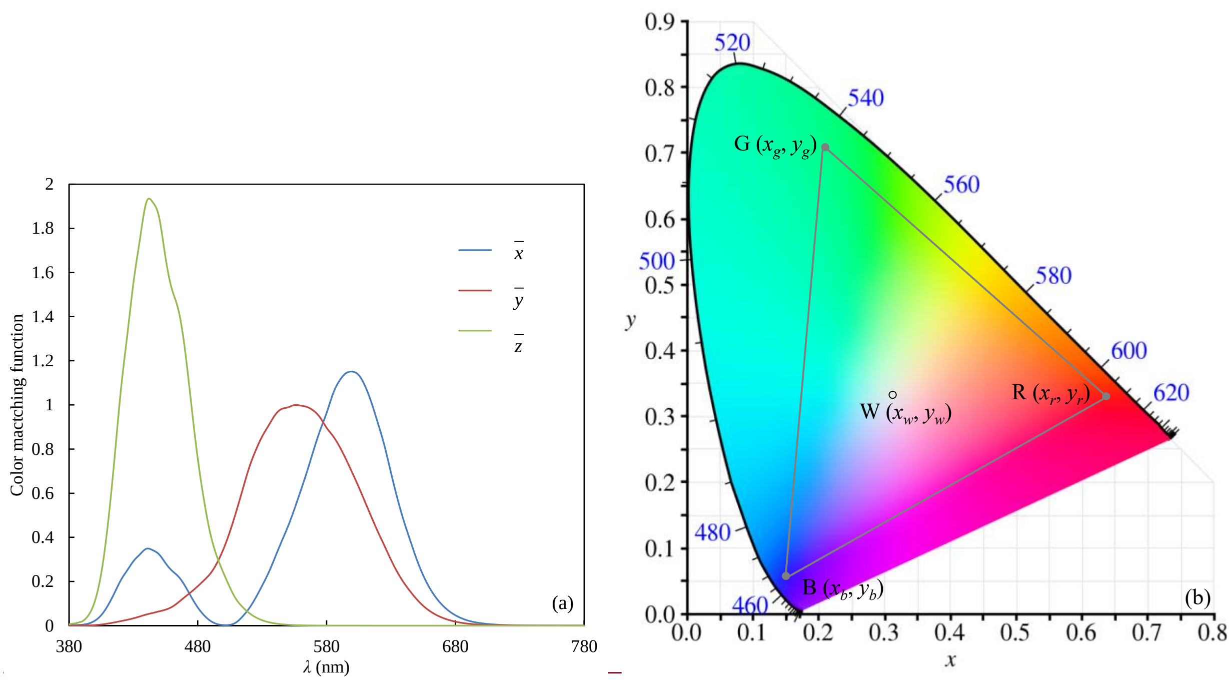

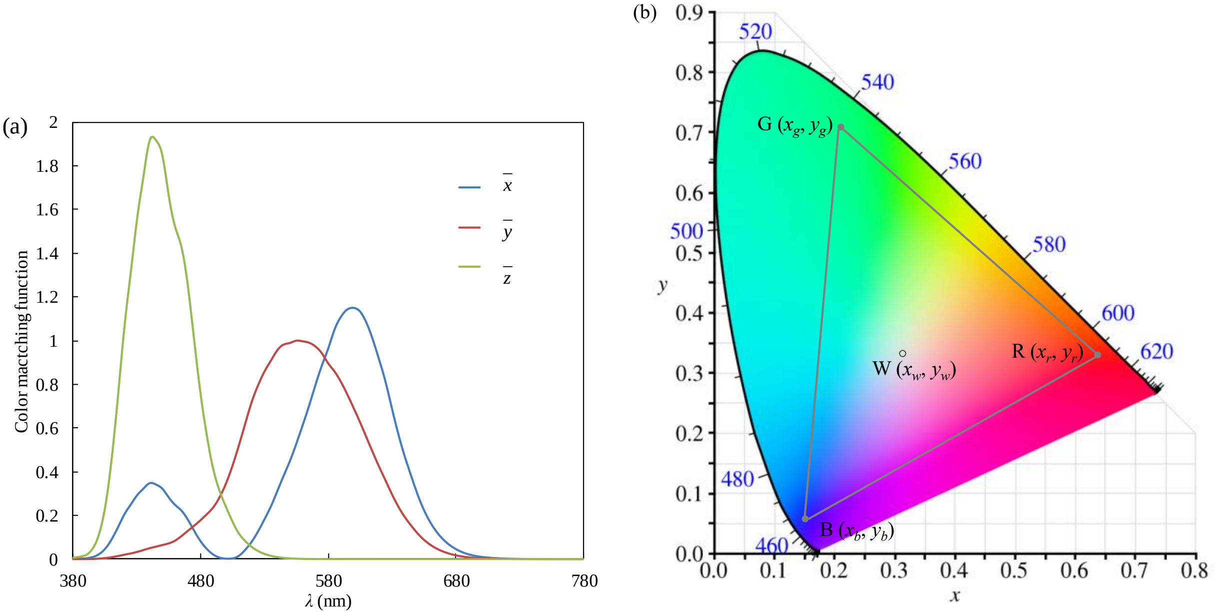

Figure 2: (a) The CIE color matching functions $\bar{x}(\lambda)$, $\bar{y}(\lambda)$, and $\bar{z}(\lambda)$, and (b) the CIE color space chromaticity diagram. The outer curved boundary is the spectral (or monochromatic) locus, with wavelengths shown in nanometers. R, G, and B are the primary colors of red, green and blue, and W is the position of the white color.

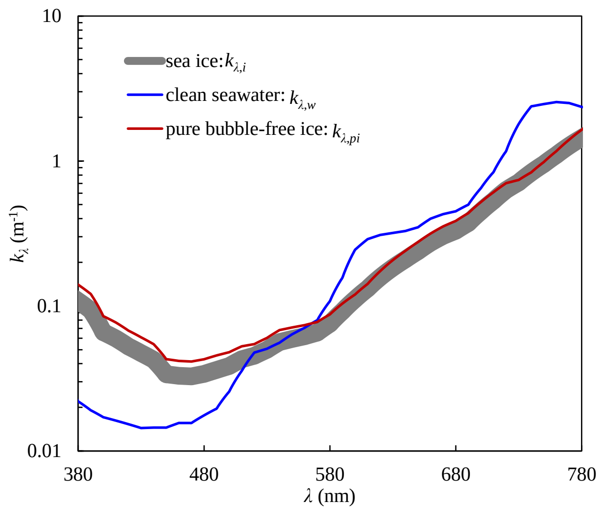

Figure 3: Absorption coefficients of clean seawater, pure bubble-free ice and sea ice in the visible band. The water data are from Smith and Baker (1981). The pure ice data are from Grenfell and Perovich (1981) and Warren (1984). The $k_{\lambda,i}$ value was calculated from $k_{\lambda,i} = v_{pi}k_{\lambda,pi} + v_{bp}k_{\lambda,w}$, based on the volume fractions $v_{pi} \geq 60\%$ and $v_{bp} \leq 20\%$ ($v_{pi} + v_{bp} \leq 100\%$) from field observations of summer Arctic sea ice (Huang et al., 2013).

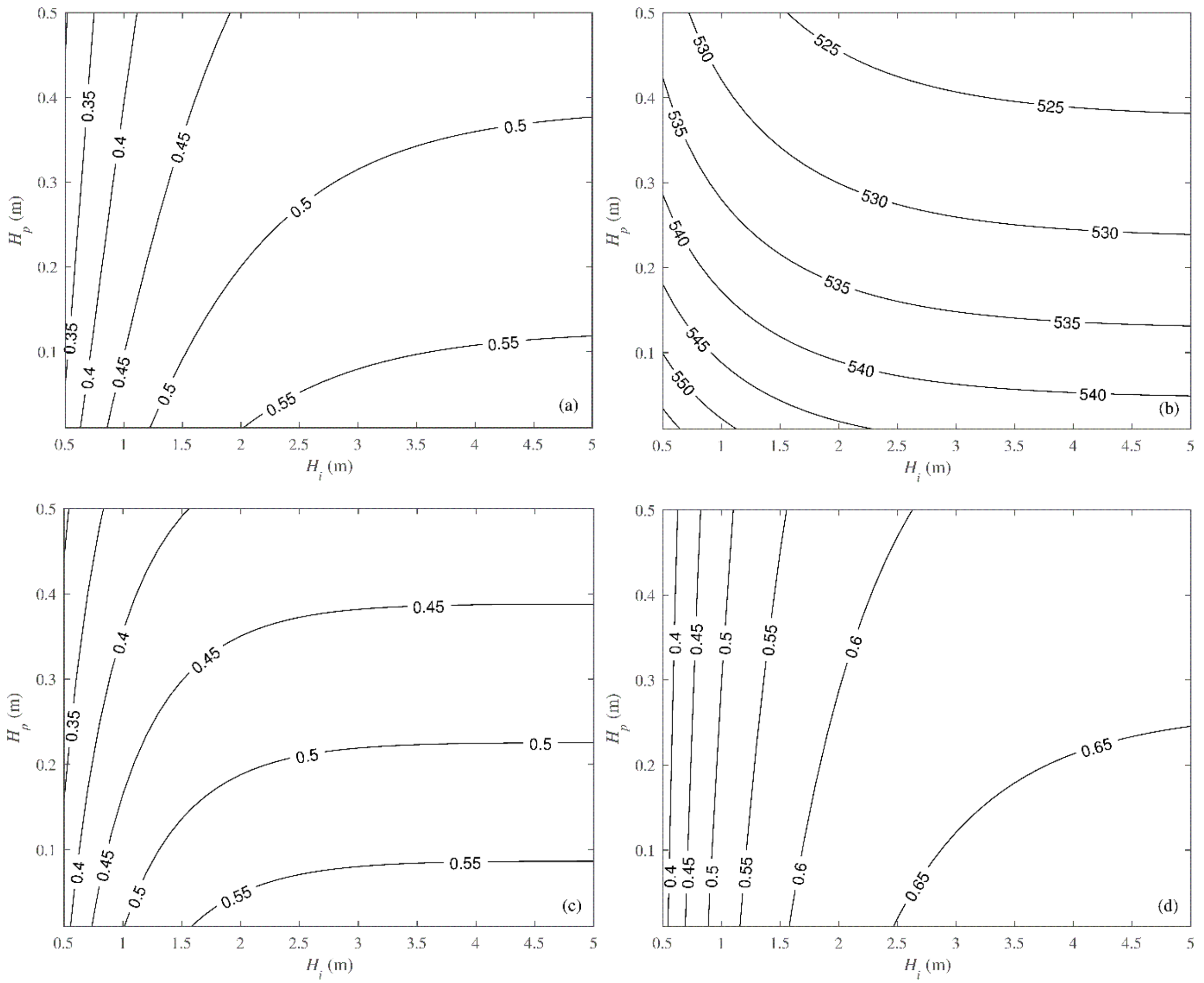
(a)
(b)
(c)
(d)
H_p (m)
H_i (m)
0.35
0.4
0.45
0.5
0.55
0.6
0.65
525
530
535
540
545
550

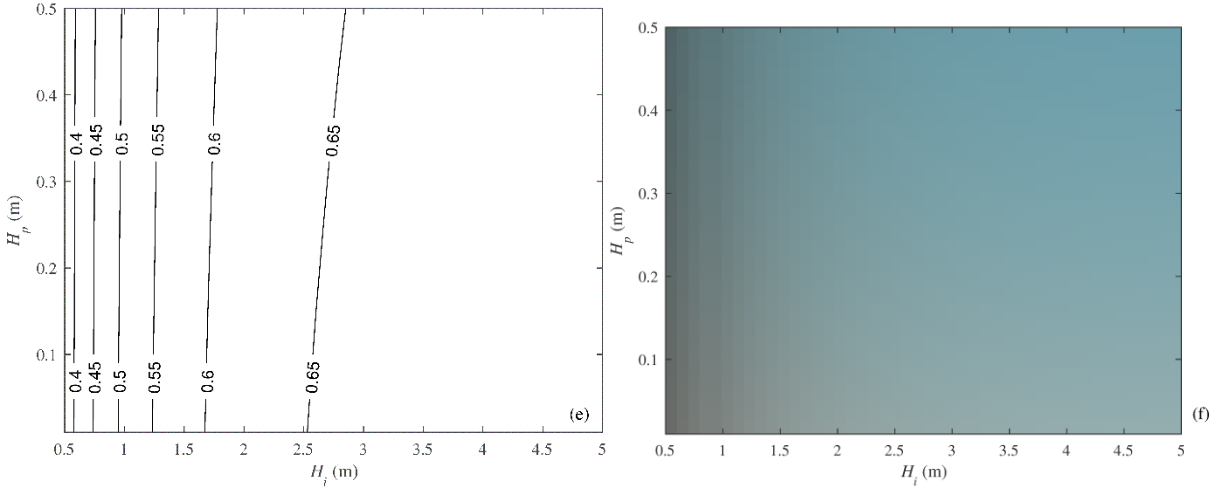
(e)
(f)
H_p (m)
H_i (m)
0.4
0.45
0.5
0.55
0.6
0.65

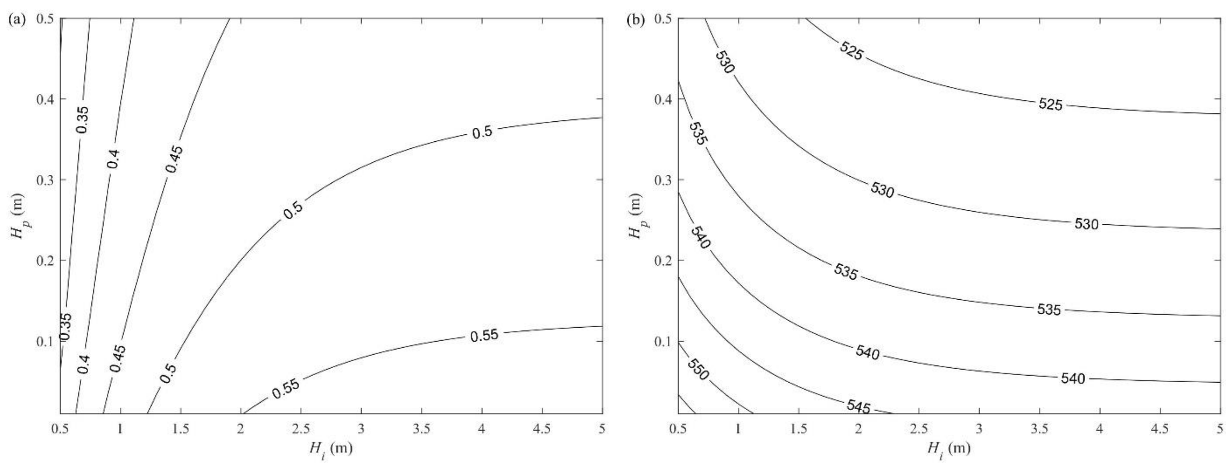
(a)
(b)
H_p (m)
H_i (m)
0.35
0.4
0.45
0.5
0.55
525
530
535
540
545
550

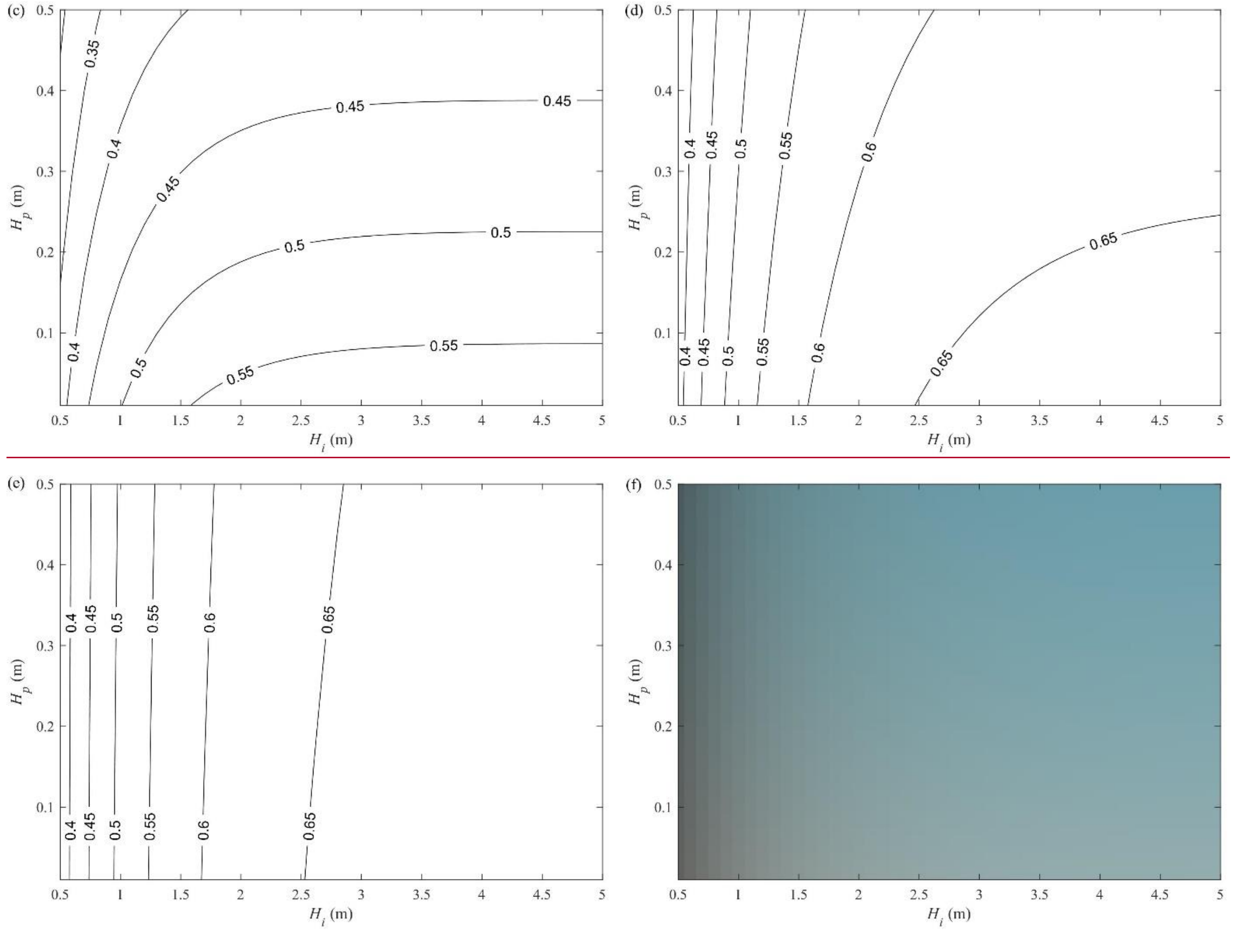

Figure 4: Variations of melt-pond optics and color with pond depth and underlying ice thickness: (a) integrated pond albedo α_B, (b) mean wavelength determined by Eq. (1), (c–e) intensities of red, green, and blue components scaled in the range of 0–1, (f) simulated color of the melt pond in the RBG color space according to the colorimetric method defined by Eqs. (2-6). The sky condition is overcast.

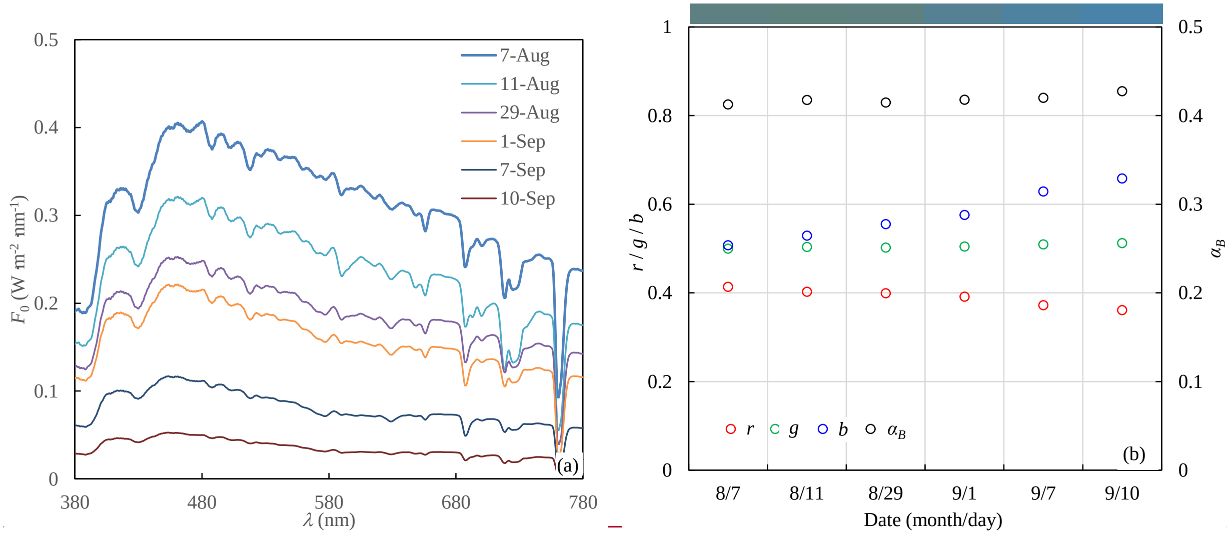

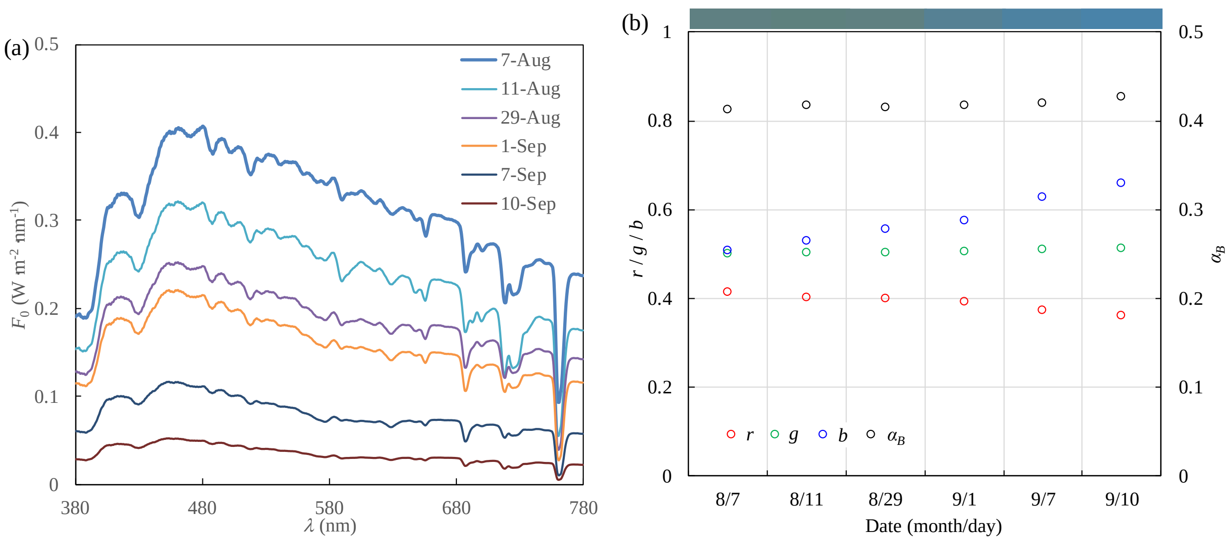

Figure 5: (a) Typical spectral incident solar irradiances in the Arctic summer under a completely overcast sky according to Grenfell and Perovich (2008), and (b) their influence on melt-pond albedo and the *rgb* intensities of pond color for H_p = 0.3 m and H_i = 1.0 m. The color bar on top of (b) denotes the simulated color of the melt pond under different sky conditions.

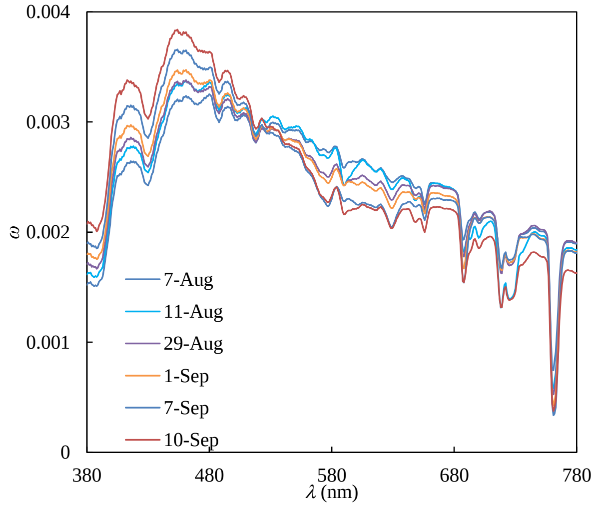

Figure 6: Normalized values of incident solar radiation under different sky conditions, defined as the ratio of the spectrum in Fig. 5a to the total energy in the visible band.

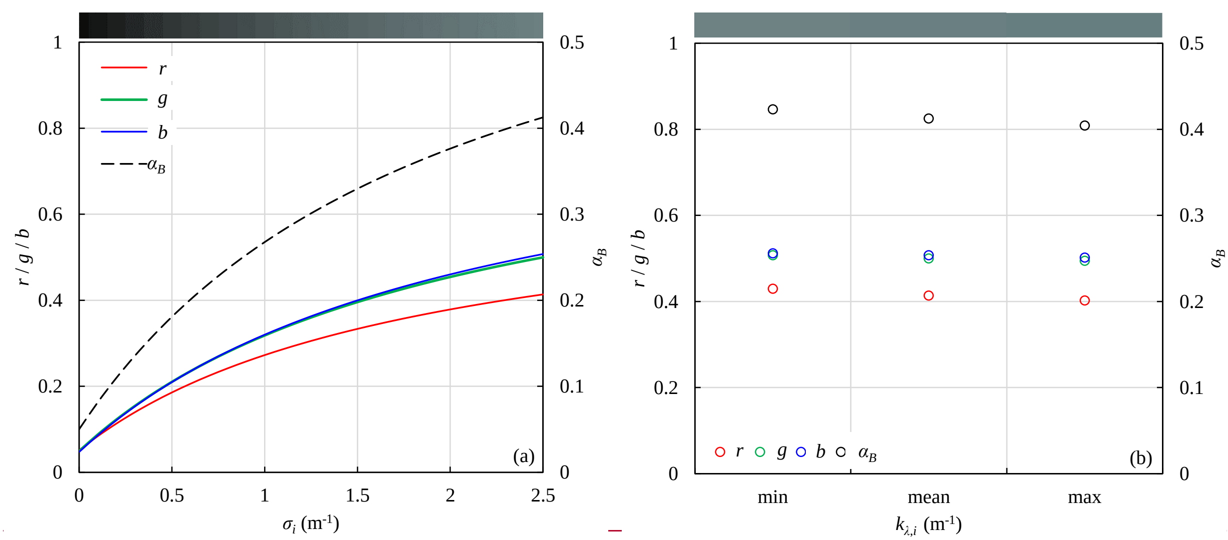

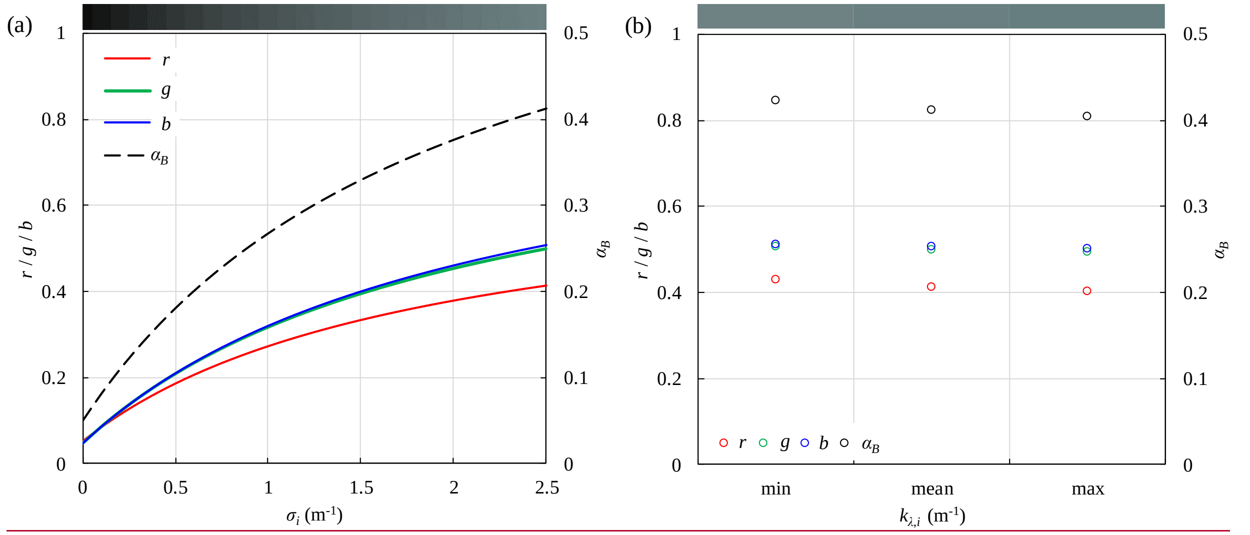

Figure 7: Variation of the *rgb* intensities of pond color and melt-pond albedo with the inherent optical properties of underlying sea ice: (a) scattering coefficient and (b) absorption coefficient for H_p = 0.3 m and H_i = 1.0 m. Note that σ_i within 1.2–2.5 m^{-1} is valid for sea ice under melt ponds, and σ_i = 0 is presented only as a comparison as an idealized purely absorbing medium. The color bar on top denotes the simulated color of the melt pond under different optical properties of sea ice.

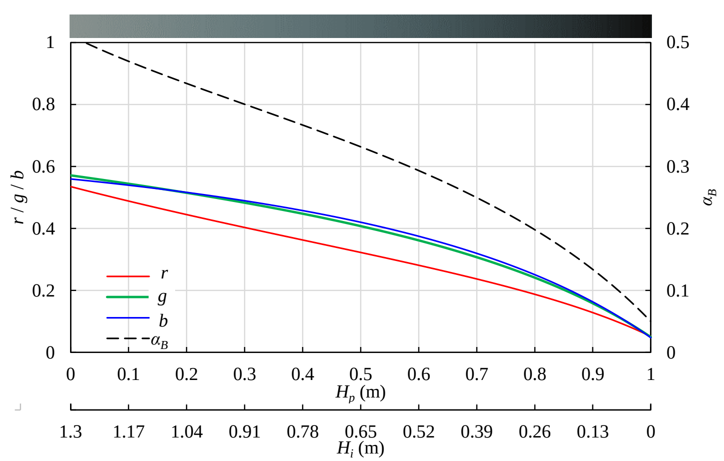

Figure 8: Variations of the *rgb* intensities of pond color and melt-pond albedo during the process of sea-ice melting, assuming H_i + δH_p = 1.3 m. The color bar on the top denotes the simulated color of the melt pond during ice melting.

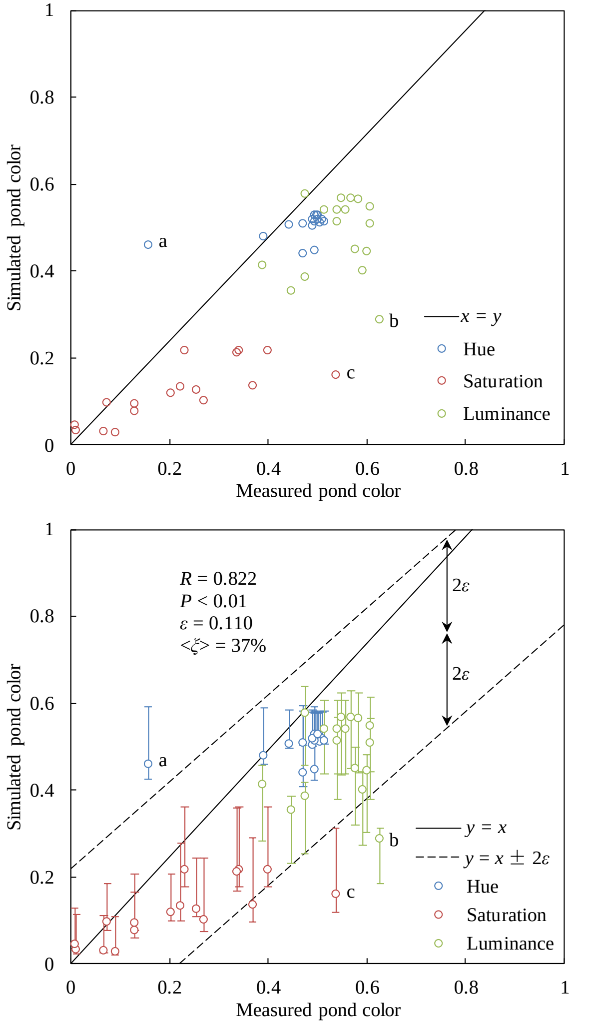

Figure 9: Comparisons of simulated pond color with in-situ measurements by Istomina et al. (2016) in the HSL color space. Points a, b, and c are special cases discussed in the text. The vertical error bars on the simulated color denote the uncertainties due to variations in the incident solar radiation and ice scattering coefficient different from their default values. *R* is the correlation coefficient between simulated and measured color. *P* is the significance level of the correlation. *ε* is the root-mean-square error, and <*ξ*> is the mean of relative error in simulated color.

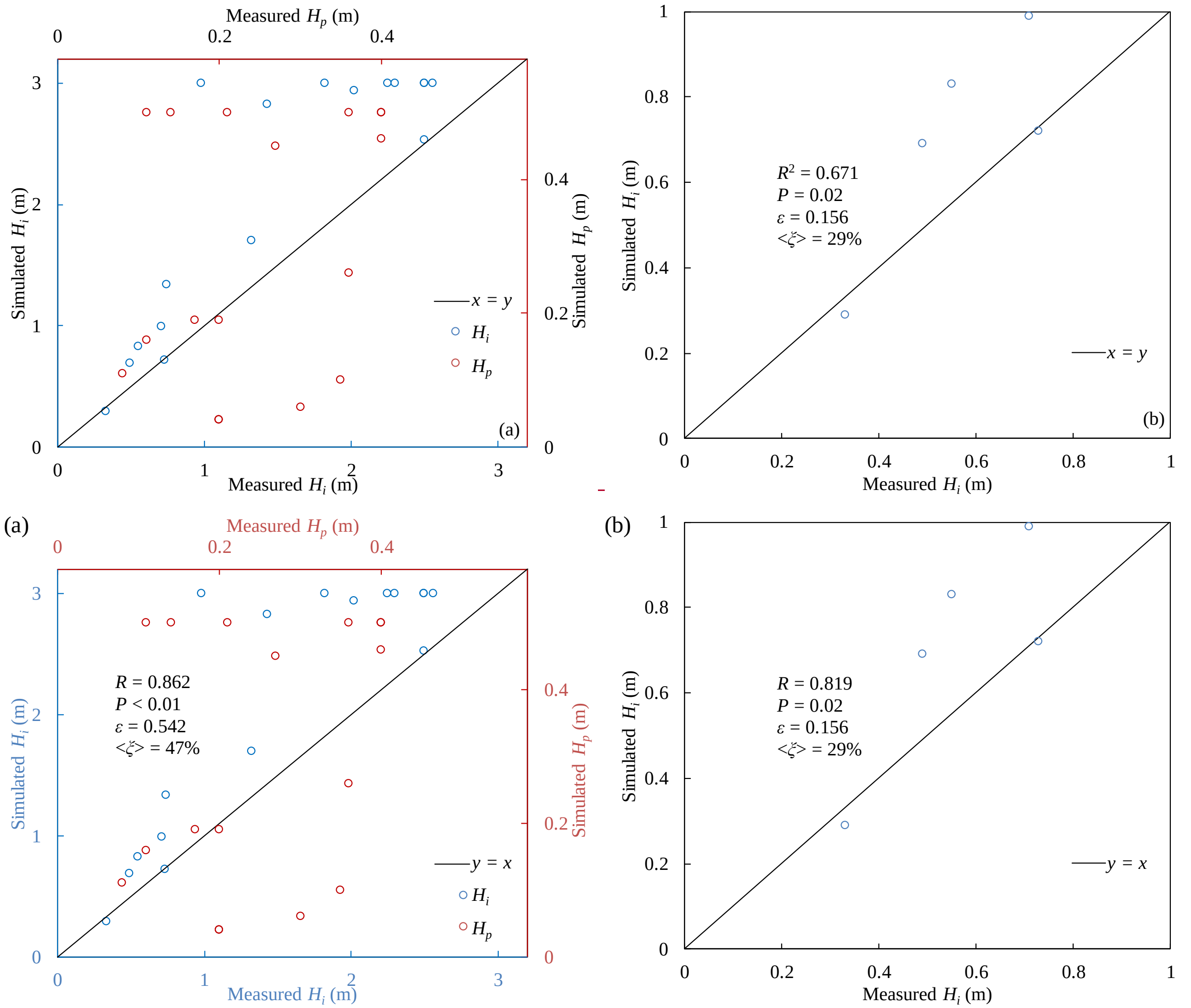

Figure 10: (a) Retrievals of underlying ice thickness and pond depth using measured pond colors in Istomina et al. (2016). (b) is a subset of (a) for H_i < 1 m. R is the correlation coefficient between simulated and measured H_i. P is the significance level of the correlation. ε is the root-mean-square error, and <ξ> is the mean of relative error in simulated H_i.